Multiple frequency microwave ablation

By

Robert W Hulsey

A Thesis
Submitted to the Faculty of
Mississippi State University
in Partial Fulfillment of the Requirements
for the Degree of Masters of Science
in Electrical and Computer Engineering
in the Department of Electrical and Computer Engineering

Mississippi State, Mississippi

May 2015

ProQuest LLC.
789 East Eisenhower Parkway
P.O. Box 1346
Ann Arbor, MI 48106 - 1346

Multiple frequency microwave ablation

By

Robert W Hulsey

Approved:

_____

Erdem Topsakal
(Major Professor)

_____

J. Patrick Donohoe
(Committee Member)

_____

Pan Li
(Committee Member)

_____

James E. Fowler
(Graduate Coordinator)

_____

Jason M. Keith
Interim Dean
Bagley College of Engineering

Name: Robert W Hulsey

Date of Degree: May 8, 2015

Institution: Mississippi State University

Major Field: Electrical and Computer Engineering

Major Professor: Dr. Erdem Topsakal

Title of Study: Multiple frequency microwave ablation

Pages in Study: 51

Candidate for Degree of Masters of Science

In recent years, microwave ablation therapy has become widely investigated as an alternative treatment to cancer. This method is one of the newest forms of ablation techniques for the removal of tumors and is minimally invasive compared to alternative treatments. One drawback to many of the current microwave ablation systems is the narrowband nature of the antennas used for the probe, such as dipole antennas. This study aims to compare ablation results of both ultra-wideband and narrowband ablation techniques. An ultra-wideband ablation probe is designed that operates from 400MHz to 2.6GHz and are compared to two designed narrowband ablation probes that operate at 915MHz and 2.4GHz, respectively. These ablation probes are tested in tissue mimicking gels and porcine liver. Provided results for this thesis will include probe designs, simulation results, and ablation experiments.

DEDICATION

This thesis work is dedicated to my fiancée, Kathryn Williams, who has been a constant source of encouragement and support during the many challenges through graduate school and life. I am truly thankful to have you in my life. This work is also dedicated to my parents, Lloyd and Sandra Hulsey, for their endless love and encouragement. In memory of my sister, Rebecca Hulsey.

ACKNOWLEDGEMENTS

I would like to express my sincerest gratitude to the many people whom have made this thesis possible, and to whom I am greatly indebted. First I would like to thank Dr. Erdem Topsakal for his teaching and guidance through my undergraduate degree, which inspired me to expand my education by pursuing my master's degree. I would also like express my appreciation to my committee members, Dr. J. Patrick Donohoe and Dr. Pan Li, for their time, support, and help with learning through the graduate program. I would like to thank Mustafa Asili for teaching me how to use several software applications and how to fabricate antennas. I would also like to thank Erin Colebeck for teaching me how to make tissue mimicking gels. Lastly, I would like to thank my family and fiancée for their constant support and inspiration.

TABLE OF CONTENTS

LIST OF TABLES

LIST OF FIGURES

CHAPTER I

INTRODUCTION

Tissue ablation has become an increasing form of research in the field of medicine, and has existed in a basic form for over a century [1]. This increase of interest comes from a rising demand for ablation techniques that are minimally invasive and inexpensive. Tumor ablation is an image guided treatment that eliminates tumors or unhealthy tissue by manipulating the target areas temperature. This can be done in several different ways, including: cryoablation, focused ultrasound ablation, laser ablation, direct current catheter ablation, radiofrequency ablation, and microwave ablation [2]. Each of the mentioned techniques work in different ways towards the common goal of eliminating unhealthy tissues without harming the surrounding healthy ones, all while being minimally invasive and relatively painless to the patient. These techniques can be used to treat a wide range of tumors in various parts of the human body such as the liver, breast, kidney, pancreas, lung, and bones [3].

Cryoablation, the oldest method of thermal ablation, utilizes nitrogen or argon gas flowing through a cryoprobe to create extremely cold temperatures as low as -75 ℃ [4]. The living tissues, healthy or unhealthy, cannot withstand these temperatures and will die from ice formations within the cells [5]. Some of the main drawbacks of cryoablation include a small lesion size and the time required to achieve an adequate result [6]. The

time required to assure the unhealthy tissue is eliminated comes from a series of repeatedly freezing and thawing the area of interest.

Focused ultrasound (FUS) ablation is a coupled system that utilizes low intensity ultrasound for imaging of the target area and high intensity ultrasound energy to increase the temperature of the targeted area. The procedure requires no incision into the body while the ultrasound energy will travel harmlessly over any overlying tissues converging to the targeted area for ablation [7]. This focused deposition of ultrasound energy produces a temperature between 65 ° - 100 ℃ using a frequency range of 2 - 20 MHz [6]. The main disadvantage of FUS ablation are the reflections at gas interfaces and its strong attenuation of bone which limits its use to areas of soft tissue. In addition to this, another disadvantage is due to the sharp focus of energy which leads to longer ablation times for larger tumors.

Laser ablation systems use a small fiber-optic probe to utilize laser energy pulses for ablating a target area [8]. The unhealthy tissue is heated by absorbing the laser energy pulses and this will evaporate the targeted area. Since 1960, when laser ablation was introduced, many different types of combinations and lasers have been studied to improve its effectiveness [2]. The biggest limitation of this system is the laser penetration through blood, which can make the procedure ineffective [8]. Laser ablation systems are also one of the most expensive options for tissue ablation.

Direct current (DC) catheter ablation systems use a catheter to utilize direct current as an energy source which would deliver a shock to the targeted area [3]. In the systems early development stages, the DC energy source was provided by a standard external defibrillator [9]. The high voltage discharge of the energy source was very

difficult to control and could potentially cause extensive tissue damage to healthy tissue outside of the targeted area's range. These disadvantages led to investigating radiofrequency ablation as an alternative, which eventually superseded DC ablation.

Radiofrequency (RF) ablation works similarly to DC ablation but uses a different energy source. This method of tissue ablation is the most commonly used due to its safety, ease of use, and effectiveness [10]. The catheter based system uses heat from high frequency alternating current in the range of 350 kHz – 1 MHz with up to 10 – 200 W of power [11]. In order for this method to work, a closed circuit is required through the use of two to four grounding pads. With RF ablation, the heating of unhealthy tissues is mainly resistive due to tissues not being a perfect conductor [12]. Due to this, the heating is only effective within a few millimeters of the tissue, so the rest of the ablation zone is created with conductive heating [14]. When the power is applied to the catheter the RF current conducted through the tissue adjacent to the electrode results in ion agitation, which causes friction that converts to heat [15]. The optimal temperature achieved for RF ablation is between 60° - 100℃ to achieve coagulative necrosis [15], [16]. Coagulative necrosis causes the tissue to become a dry, homogenous eosinophilic mass due to the coagulation of protein. Even though RF ablation is the most commonly used method of tissue ablation, there are major disadvantages. The procedure relies on the conduction of electrical current into the tissue, which limits its uses to a single probe. The electrical energy causes a rapid increase in temperature and ablation size, but starts to decrease as the temperature reaches 100 ℃ due to the leaving of water from the tissue. This decrease is a result of an impedance rise and the decay rate of power [17], [18], [19]. The change in impedance as temperature increases is shown in Figure 1.1 [13]. In addition to this,

another disadvantage of this system is from the discomfort of the procedure due to the resistive heating of the ground pads. Resistive heating from the system will result in skin burns where the ground pads are attached [20].

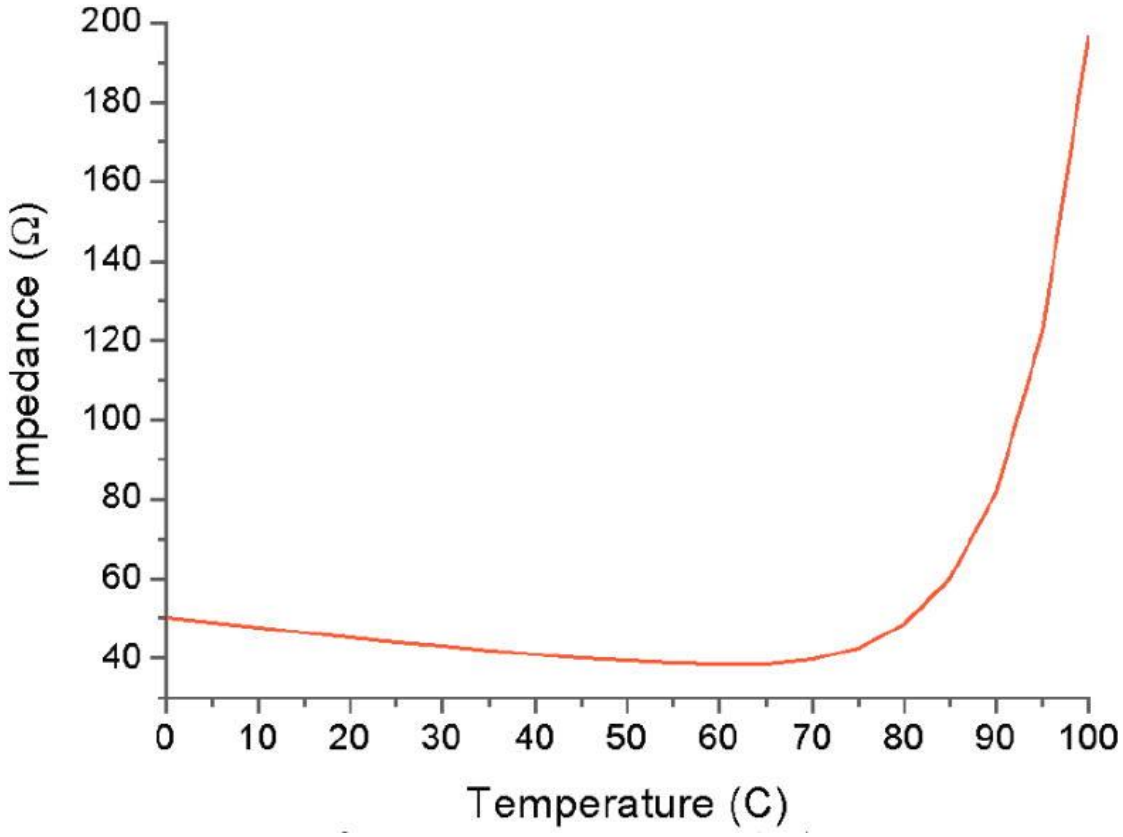

Figure 1.1 Impedance vs. temperature for RF ablation.

The drawbacks of these systems have resulted in the investigation of alternative procedures that would maintain a high success rate while reducing the limitations of tissue ablation. Microwave (MW) ablation is the newest technique developed for tissue ablation and is similar to RF ablation [16]. The majority of clinical trials for MW ablation to examine the efficiency and safety comes from Japan, where the first MW ablation

procedure was performed in 1990 at 2.4 GHz [2]. In 2003, the US performed its first procedure with MW ablation using a newly developed 915 MHz system [21]. The most common frequency band allowed by the Federal Communications Commission (FCC) to operate MW ablation systems is from 915 MHz to 2.45 GHz. There are several potential advantages to MW ablation systems compared to RF ablation systems. One of the main advantages include a more consistent production of high temperature in the tissues. MWs can focus energy more directly into the tissue due to shorter wavelengths than RF systems [16]. The focused energy of the MW system allows for faster ablation times and larger ablation volumes, which results in less procedural pain. MW systems are also not limited to a single probe or a grounding pad. A MW ablation system setup is made up of three main parts including an imaging system, thermometry system, power source (MW generator), and MW antenna catheter. The equipment for this setup is shown in Figure 1.2, where (left) represents a triple probe system, (middle) represents a MW generator, and (right) represents the imaging system [22], [23].

Figure 1.2 MW ablation system

MW ablation systems work under the electromagnetic (EM) propagation principle by using EM waves to increase the temperature of the targeted tissue area at a quick rate homogeneously [24]. The water molecules in the tissue begin to oscillate positive and negative charges when exposed to EM radiation, which causes cell death due to the increased heat. MW effect on water molecules is shown in Figure 1.3 [25].

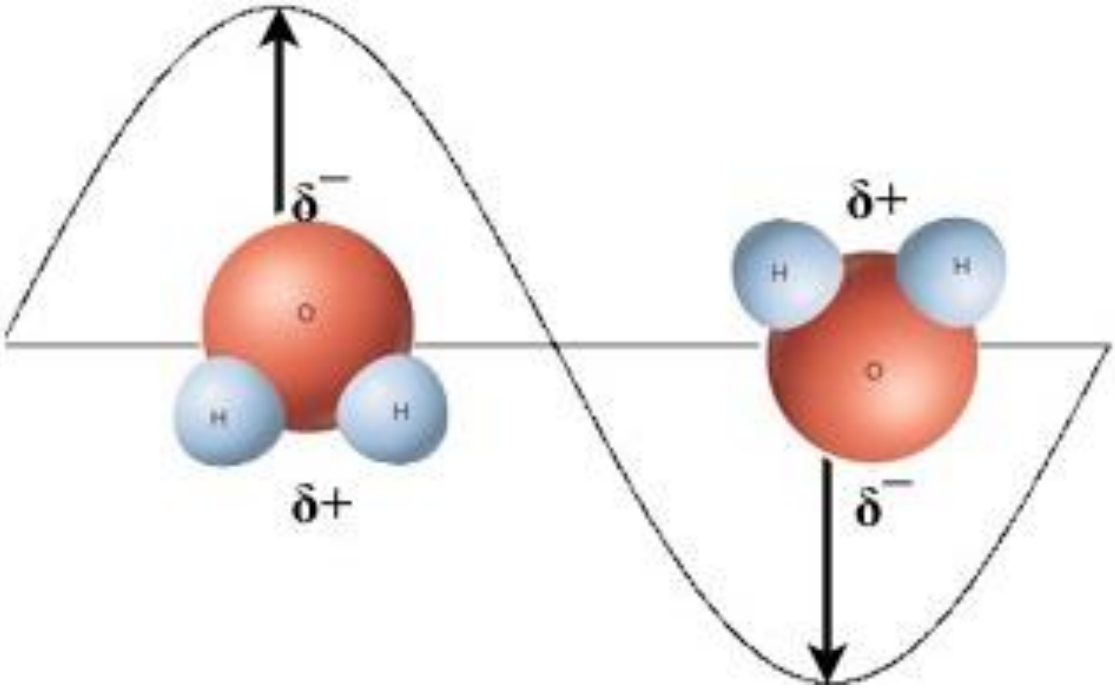

Figure 1.3 MW effect on water molecules

One of the major advantages of a MW ablation system compared to an RF ablation system is that MWs can provide a more uniform ablation zone. This is primarily due to the power deposition decay being slow at high temperatures [16], [26], shown in Figure 1.4 [27]. Figure 1.4 provides results of RF ablation at 200W input power in conjunction with MW ablation at 60W input power and the resulting temperature increase

5mm away from the ablation probe at 2.45 GHz. The results of this figure show that as time and temperature increase, RF ablation temperature levels slowly increase compared to MW ablations rapid and steady ablation.

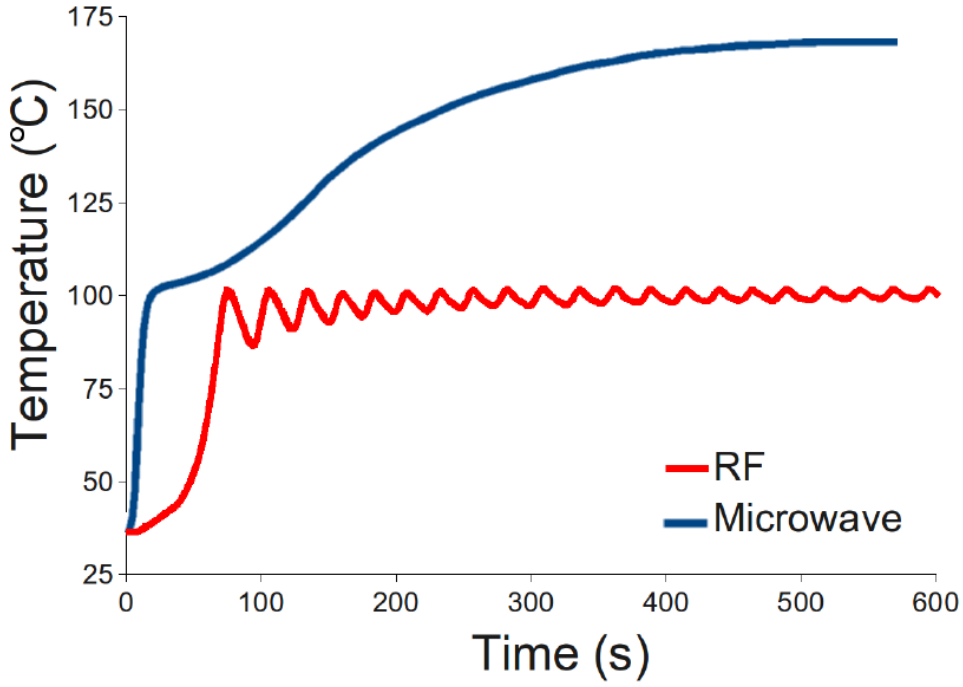

Figure 1.4 Increase in temperature over time of MW and RF systems

RF ablation systems rely on conductivity and controlled temperature to achieve a desired result of ablation. The temperature must be controlled to account for the impedance change and prevent charring damage to the tissue. MW ablation systems are able to provide a substantial temperature increase regardless of the impedance change [28]. MWs are also able to propagate through tissue regardless of the tissues conductivity [13].

Many MW ablation systems today show several benefits in comparison to RF ablation, however there are disadvantages to these systems. The biggest disadvantage to these systems is impedance matching. The antennas used for MW ablation must be impedance matched to the feed line for effective results. As the tissue properties are changing during the ablation process, the resonating frequency of the antenna will begin to shift to another frequency range due to temperature increase and evaporation of water molecules. Most of the current MW ablation systems only resonate at one frequency, typically 915 MHz or 2.4 GHz, which is mainly due to the designed antenna being narrowband [29]. Depending on the ablation zone required, many systems use 2-3 different applicators which resonate at different frequencies. If these systems were to use only one resonating frequency, as the impedance changes and the frequency begins to shift, the return loss and power reflection will begin to increase. In this study, two narrowband antenna applicators are designed for MW ablation and compared to a previously developed ultra-wideband antenna applicator from Mississippi State University [27]. The ablation tests are performed in porcine liver, tissue mimicking dielectric gel, and results are provided. The two narrowband antenna applicators are designed using High Frequency Structure Simulator (HFSS), while considering the tissues dielectric properties. Provided in this study is the theory and design of MW antennas with presented measurements on return loss with and without temperature effects, gain patterns, and specific absorption rate (SAR) values. Lastly, these results are validated using ex vivo porcine liver experiments.

CHAPTER II

THEORY AND DESIGN OF MICROWAVE ANTENNA APPLICATORS

2.1 Antenna Applicator Theory

The purpose of this study is to develop two narrowband antenna applicators that are designed for the use of tissue ablation. Both of the antenna applicators have a microwave antenna printed at the end of the substrate. Antenna basics are considered during the development of these applicators. The Institute of Electrical and Electronics Engineers (IEEE) states that the definition of an antenna is: "The part of a transmitting or receiving system that is designed to radiate or receive electromagnetic waves" [30].

Antennas work by using an oscillating charge distribution to produce electromagnetic radiation. The two main types of antennas are transmitting, which converts an electrical signal into waves, and receiving, which takes a transmitted wave and converts it into an electrical signal. In this study, we focus on transmitting antennas. As the antenna accelerates or decelerates the motion of charge, a radiation occurs. Electromagnetic radiation refers to the strength and direction of waves propagating from the antenna. This radiation can potentially occur in three regions around the antenna. The three different regions are described as the far field or Fraunhofer region, the reactive near field, and the radiating near field (Fresnel region) [31].

The far field region is described as the region farthest away from the antenna. In this region, the distance does not affect the radiation pattern. This region is primarily

dominated by radiated regions with the corresponding E and H regions being orthogonal to one another. The propagation direction is in the direction of the plane waves. In order to be in the far field, the equations below must be satisfied [20].

$$R > \frac{2D^2}{\lambda} \quad \text{(Eq. 2.1)}$$

$$R \gg D \quad \text{(Eq. 2.2)}$$

$$R \gg \lambda \quad \text{(Eq. 2.3)}$$

In these equations R is the radius of the field (m), D is the maximum dimension of the antenna (m), and λ is the wavelength (m). Equation 2.1 and Equation 2.2 ensure that the power that is being radiated from certain parts of the antenna, in a given direction, are approximately parallel to one another. Equation 2.3 ensures that the reactive regions have died off and that we are left with only radiating regions.

The reactive near field region is located in the region closest to the antenna. A reactive near field can be described as a field that's E and H regions are out of phase from one another, which is dependent on distance and direction from the antenna. This region is bound mathematically by Equation 2.4 [20].

$$R < 0.62\sqrt{\frac{D^3}{\lambda}} \quad \text{(Eq. 2.4)}$$

Since the reactive near field is primarily where the reactive regions take place, this region will react to absorption [32].

The radiating near field is located in between the far field and the reactive near field. This region is primarily radiating regions, where the shape of the radiation pattern

may change depending on varying distances. This region is primarily bound by equation 2.5 [20].

$$0.62\sqrt{\frac{D^3}{\lambda}} < R < \frac{2D^2}{\lambda} \qquad \text{(Eq. 2.5)}$$

Depending on the value of R and the wavelength in this equation, this region can potentially be non-existent. Finally, these regions are show in Figure 2.1 [33].

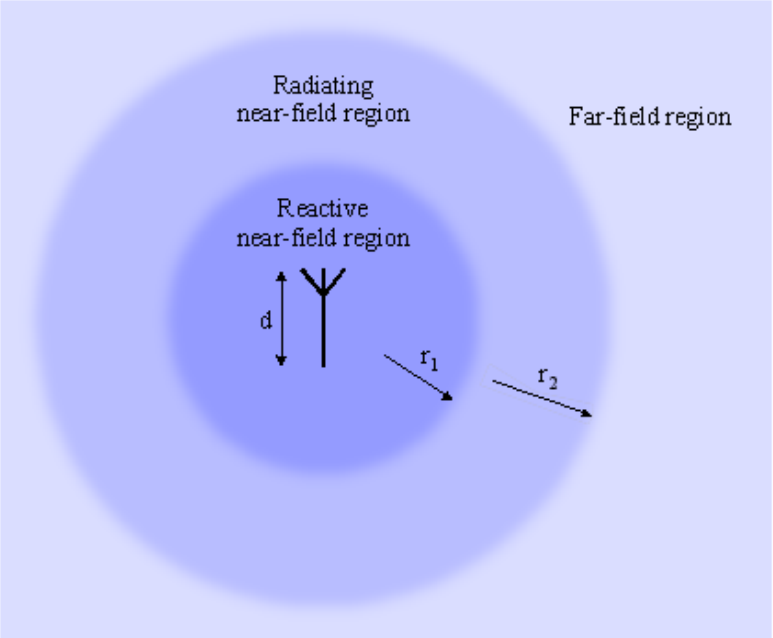

Figure 2.1 Field Regions around an Antenna

In the reactive and radiating field regions the E and H region attenuate at $1/R^3$ and $1/R^2$, and eventually dissipate with 1/R in the far field region [31]. This suggests that radiation cannot occur for extended periods of time in the near field due to loss characteristics of medium limits in the ablation zone. This disadvantage of MW ablation applicators limits the ablation zone due to EM waves not being able to penetrate more

than a few centimeters. The penetration depth is also affected by an increasing medium density in comparison to air. As the relative permittivity of the medium increases, a decrease in the wavelength occurs [29]. This disadvantage can be shown in the following Equation 2.6 – Equation 2.9. In these equations μ_0 is the vacuum permeability, ε_0 is the vacuum permittivity, μ_r is the relative permeability, ε_r is the relative permittivity, c is the speed of light in the vacuum, v is the speed of light in the medium, λ is the wavelength, and f is the frequency of the antenna.

$$\mu_0\varepsilon_0 = {}^{1}/_{c^2} \quad \text{(Eq. 2.6)}$$

$$\mu\varepsilon = {}^{1}/_{v^2} \quad \text{(Eq. 2.7)}$$

$$\mu = \mu_0\mu_r\,,\ \varepsilon = \varepsilon_0\varepsilon_r \quad \text{(Eq. 2.8)}$$

$$\lambda = {}^{c}/_{f} \ \ or \ \ \lambda = {}^{v}/_{f} \quad \text{(Eq. 2.9)}$$

Another important parameter in the design of MW ablation applicators is the bandwidth (Hz). The bandwidth can be described as a range of frequencies in which an antenna can efficiently radiate. Narrowband and wideband antennas are different from each other in terms of bandwidth. For narrowband antennas, bandwidth is the percentage difference of the highest frequency (f_H) and lowest frequency (f_L) divided by the central frequency (f_C) [34]. This percent bandwidth is mathematically represented by Equation 2.10. Many of the current ablation systems use narrowband antenna applicators such as dipole or slot antennas. Figure 2.2 shows the narrowband nature of a current slot antenna applicator used for tissue ablation [27]. The reflection coefficient (S11), or return loss, is shown to determine the bandwidth. This S11 represents how much power is being

reflected back to its source and how much power is being delivered to the antenna in a certain bandwidth.

$$BW_n = \left[\frac{f_H - f_L}{f_C}\right] 100 \qquad \text{(Eq. 2.10)}$$

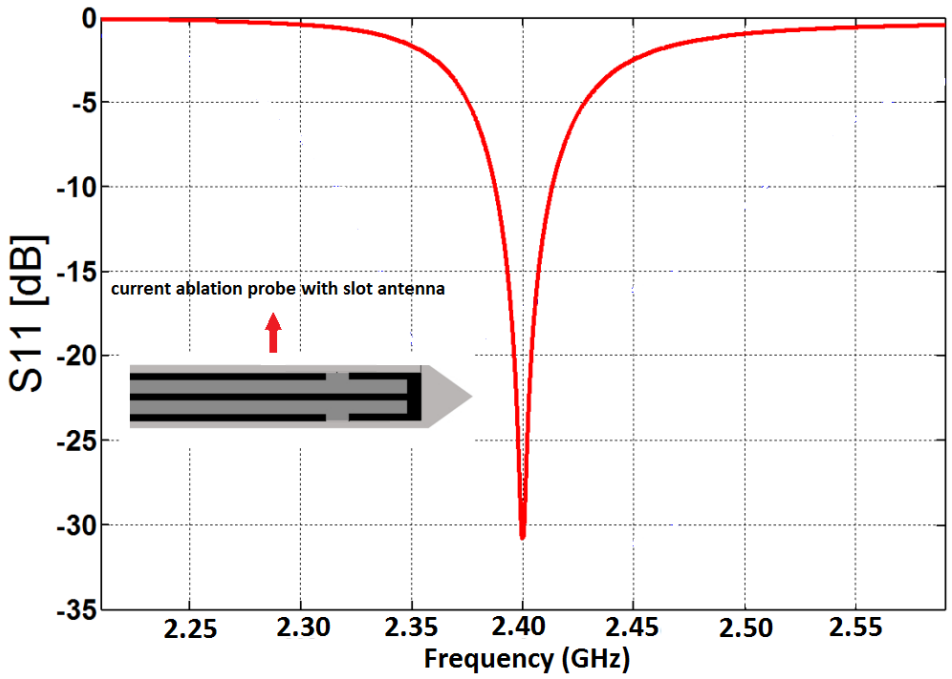

Figure 2.2 Return loss (s11) of slot antenna applicator

For antennas, the bandwidth is a ratio of the upper and lower frequency of the desired frequency range. In order for an antenna to be considered wideband, the upper frequency must be two times larger than the lower frequency [35]. The mathematical representation of bandwidth for a broad band antenna is shown in Equation 2.11. The bandwidth of the ultra-wideband applicator used in this study is shown in Figure 2.3 [27].

$$BW_b = \frac{f_H}{f_L} \qquad \text{(Eq. 2.11)}$$

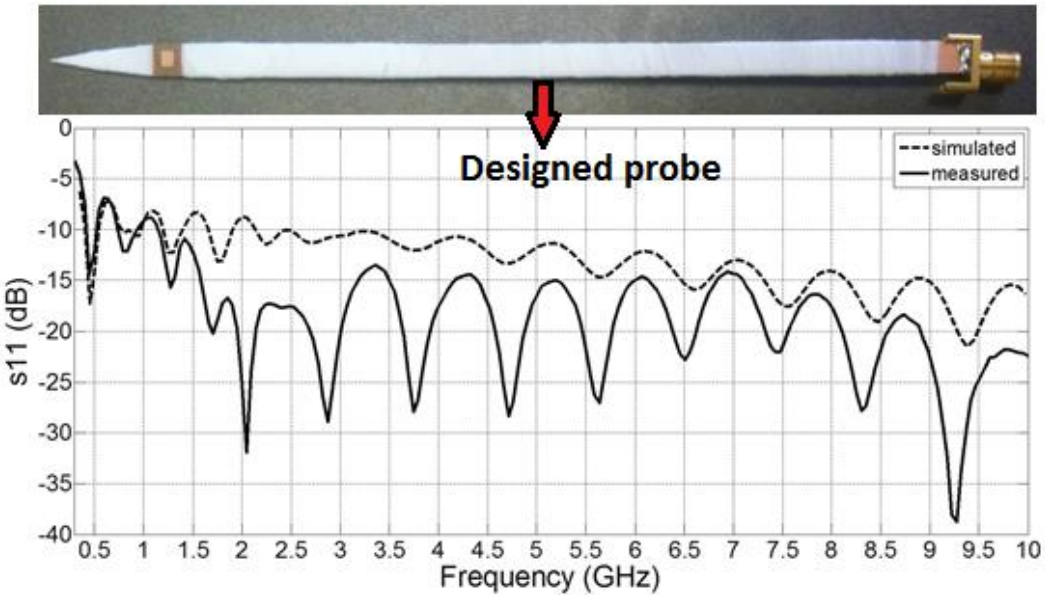

Figure 2.3 Return loss (s11) of ultra-wideband antenna applicator

The final parameter considered in the design of these microwave ablation applicators is the reflection coefficient (Γ). The reflection coefficient can be described as the amplitude of forward travelling waves compared to the amplitude of backwards travelling waves. The mathematical representation of reflection coefficient is show in Equation 2.12 [29].

$$\Gamma = \frac{Reflected\ wave}{Incident\ wave} = \frac{Z_L - Z_0}{Z_L + Z_0} \qquad \text{(Eq. 2.12)}$$

In this equation Z_0 and Z_L are the characteristic impedance of the feed line and load used in the system. This equation suggests that as the load changes, the reflection coefficient will change as well. This change of the reflection coefficient affects power transmission. The return loss, described as S11, is a function of the reflection coefficient shown in Equation 2.13 [34].

$$S_{11} = 20 \log \Gamma \qquad \text{(Eq. 2.13)}$$

In this study, a coaxial cable is used in conjunction with a liver impedance to efficiently match the designed antennas. A diagram of the reflection coefficient in a transmission line with a load (ablation probe in liver environment) is shown in Figure 2.4 [27].

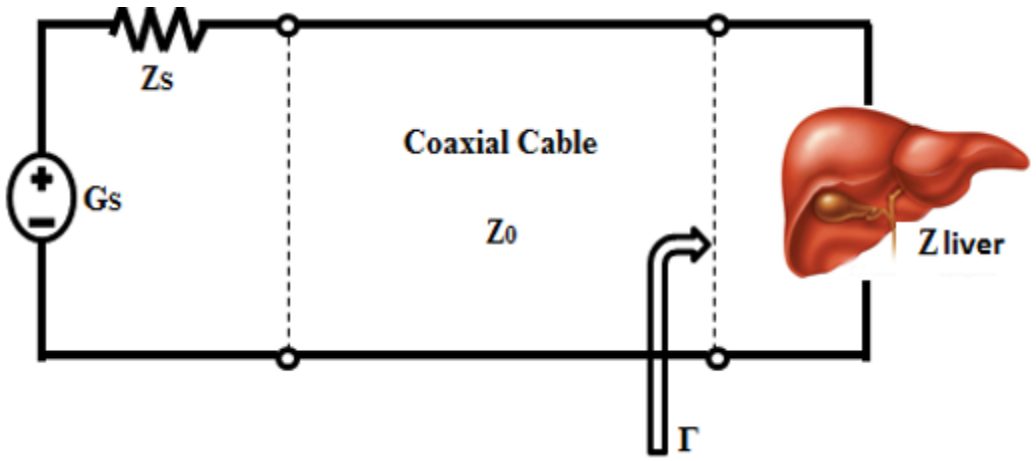

Figure 2.4 Reflection coefficient in transmission line with load (liver)

In this figure G_S is the power source, Z_S is the source impedance, and Z_0 is the characteristic impedance of the coaxial cable. One issue with MW ablation systems is tail heating due to impedance mismatch, so it is important to take the parameter equations into account when designing an antenna for the purpose of tissue ablation. Improper impedance matching of the antenna applicator can result in undesirable ablation zones or tail heating inside of the tissue. Undesirable ablation zone produced by impedance mismatch is shown in Figure 2.5 [38].

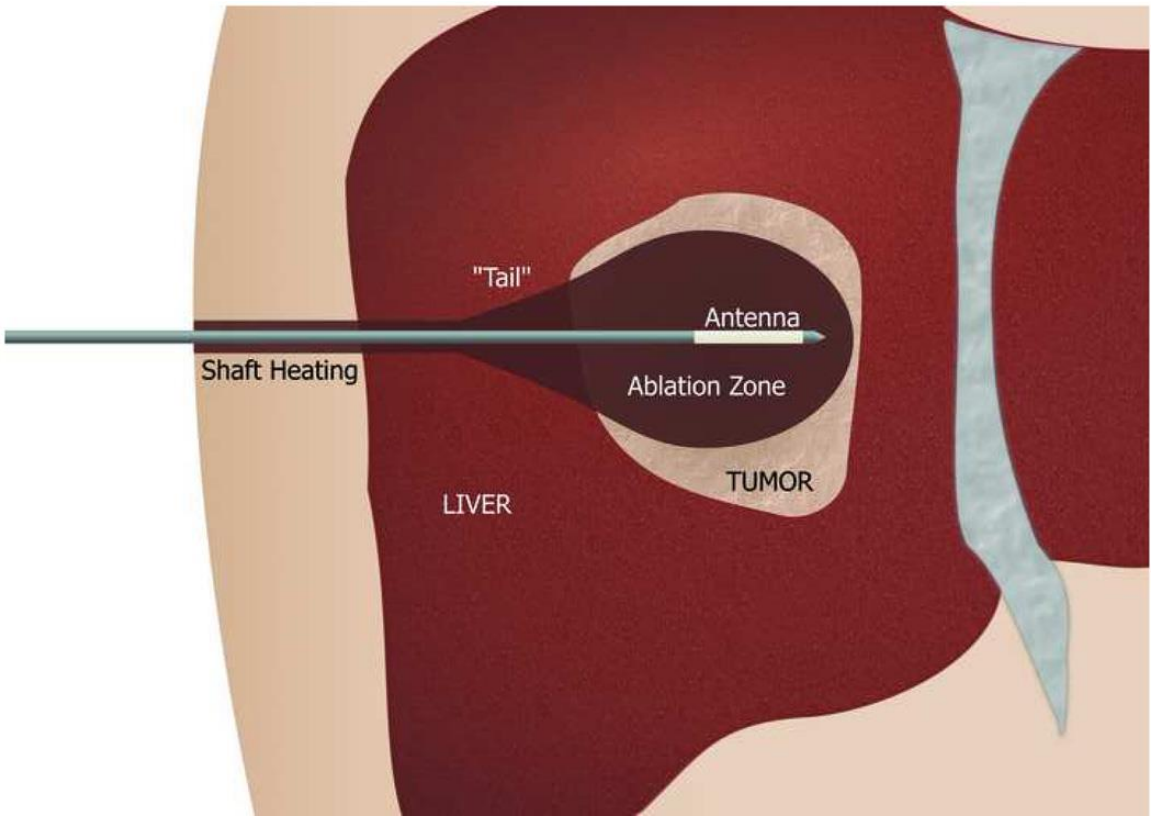

Figure 2.5 Undesirable ablation zone produced by impedance mismatch

2.2 Microwave Ablation Applicator Design

In this study, two narrowband antenna applicators are designed using HFSS software to be compared to an ultra-wideband antenna applicator. The designed antennas operate at 915 MHz and 2.4 GHz, respectively. During the design of the two antennas, liver is used as the dielectric medium to ensure an efficient design. At 915 MHz, liver conductivity (0.86121 S/m) and relative permittivity (ε_r = 46.764) values are given to the dielectric medium in the design [37]. The designed antennas and dielectric medium is shown in Figure 2.6 where (a) represents the 915 MHz applicator and (b) represents the 2.4 GHz applicator, and Figure 2.7, respectively.

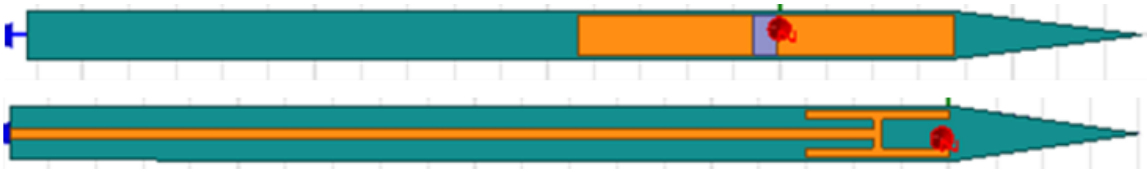

Figure 2.6 Antenna views in HFSS

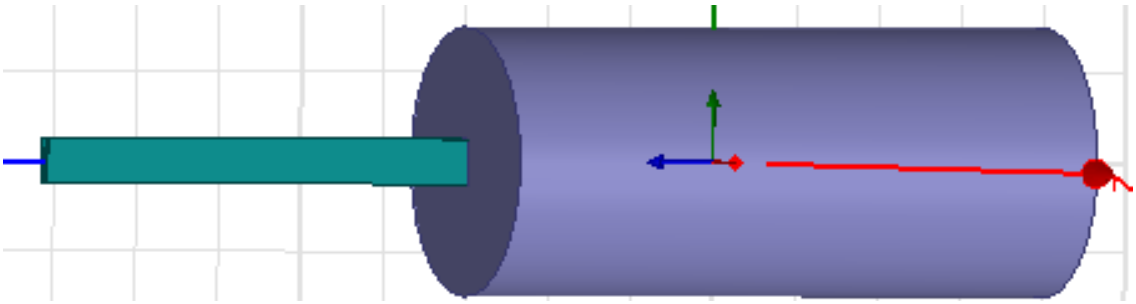

Figure 2.7 Designed antenna in dielectric medium (liver)

Many current systems utilize a dipole antenna for ablation systems. The dipole antenna on the tip of the applicator is designed with the dipole arm length of a quarter-wavelength. Provided in Equation 2.14 and Equation 2.15 where L is the length of the antenna, C is the speed of light, f is the frequency, and λ is the wavelength (m). The geometry and dimensions of the 915 MHz designed antenna are shown in Figure 2.8 and Table 2.1, respectively. In this figure, the copper is represented with the color black and the ground is shown in the bottom view.

$$\lambda = \frac{C}{f} \quad \text{(Eq. 2.14)}$$

$$L = \frac{1}{4}\lambda \quad \text{(Eq. 2.15)}$$

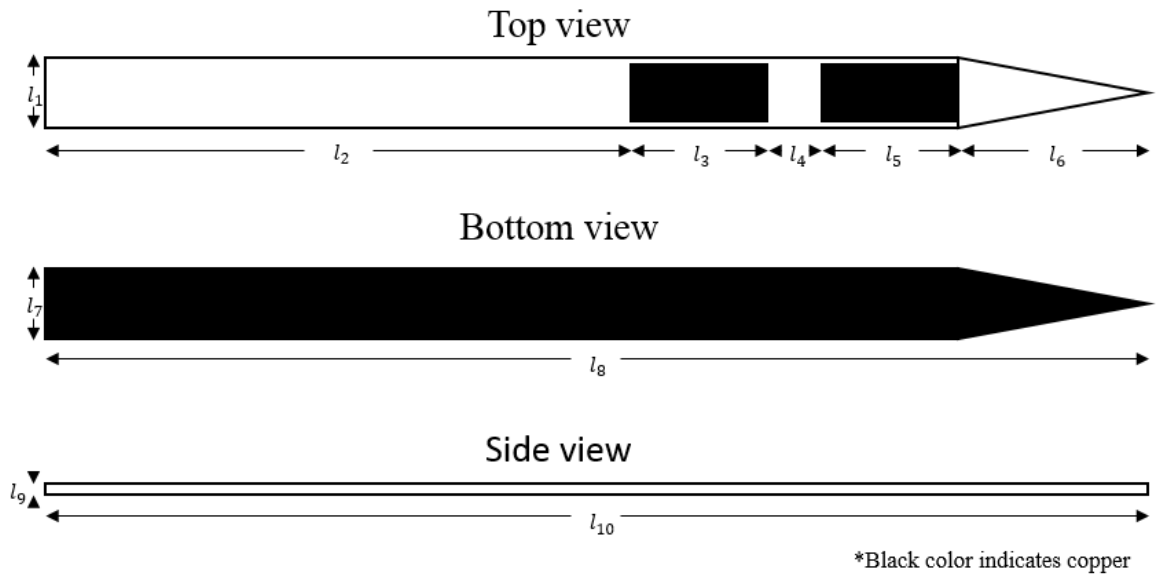

Figure 2.8 915 MHz designed antenna geometry

Table 2.1 915 MHz designed antenna dimensions

Symbol	Dim.(mm)	Symbol	Dim.(mm)
l_1	5.5	l_6	20
l_2	79	l_7	5.5
l_3	9	l_8	120
l_4	3	l_9	1.5
l_5	9	l_{10}	120

The 2.4 GHz antenna was designed similarly to the 915 MHz antenna, given the same applicator size with the same dielectric medium (liver). The dielectric medium values had to be adjusted for 2.4GHz with a conductivity of 1.6534 S/m and a relative permittivity of 43.118 [37]. Each antenna is designed using a Rogers RO2010 substrate with a dielectric constant (□r) equal to 10.2. The geometry and dimensions of the 2.4

GHz designed antenna are shown in Figure 2.9 and Table 2.2, respectively. In this figure, the copper is represented with the color black and the ground is shown in the bottom view.

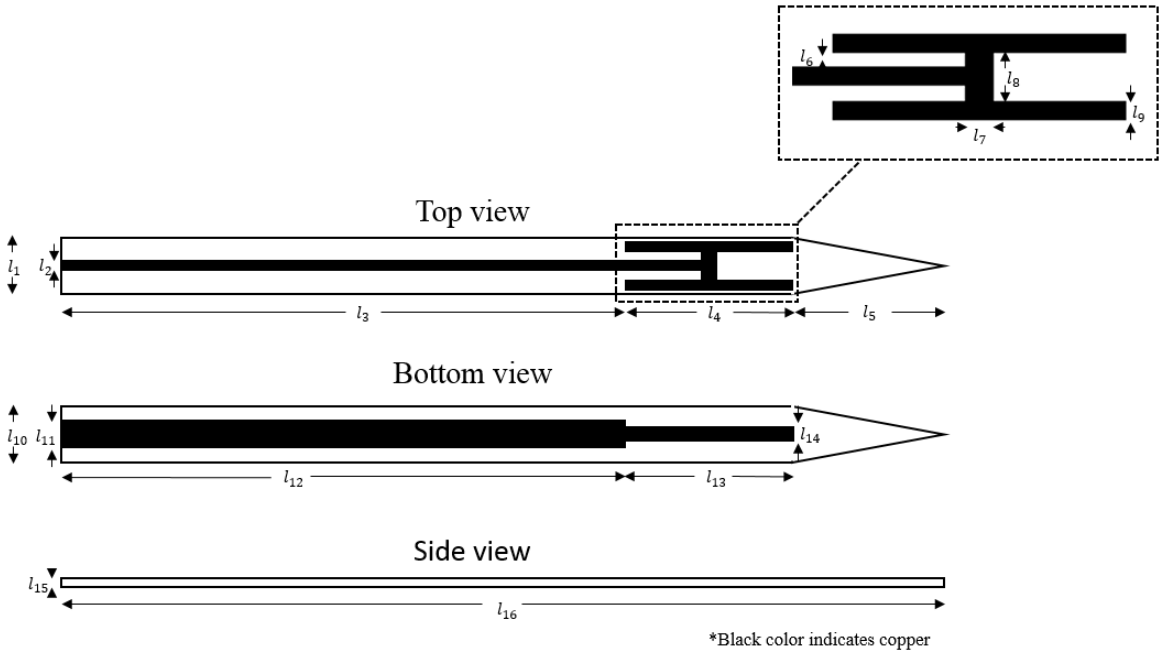

Figure 2.9 2.4 GHz designed antenna geometry

Table 2.2 2.4 GHz designed antenna dimensions

Symbol	Dim.(mm)	Symbol	Dim.(mm)
l_1	5.5	l_9	1
l_2	1	l_{10}	5.5
l_3	91	l_{11}	3
l_4	9	l_{12}	91
l_5	20	l_{13}	9
l_6	1	l_{14}	2
l_7	1	l_{15}	1.5
l_8	3	l_{16}	120

2.3 Simulation Results

Ansys HFSS is used to simulate the designed applicators in various settings. Each applicator is simulated in a liver medium encased in an air box with dimensions calculated from Equation 2.14 and Equation 2.15. Simulated bandwidth results for the 915 MHz and 2.4 GHz antenna applicators are shown in Figure 2.10 and Figure 2.11, then compared to the simulated results of the ultra-wideband applicator in Figure 2.12 [27]. Figure 2.13 and Figure 2.14 provide the antenna gain pattern values of each antenna applicator compared to the ultra-wideband applicator in Figure 2.15 [27].

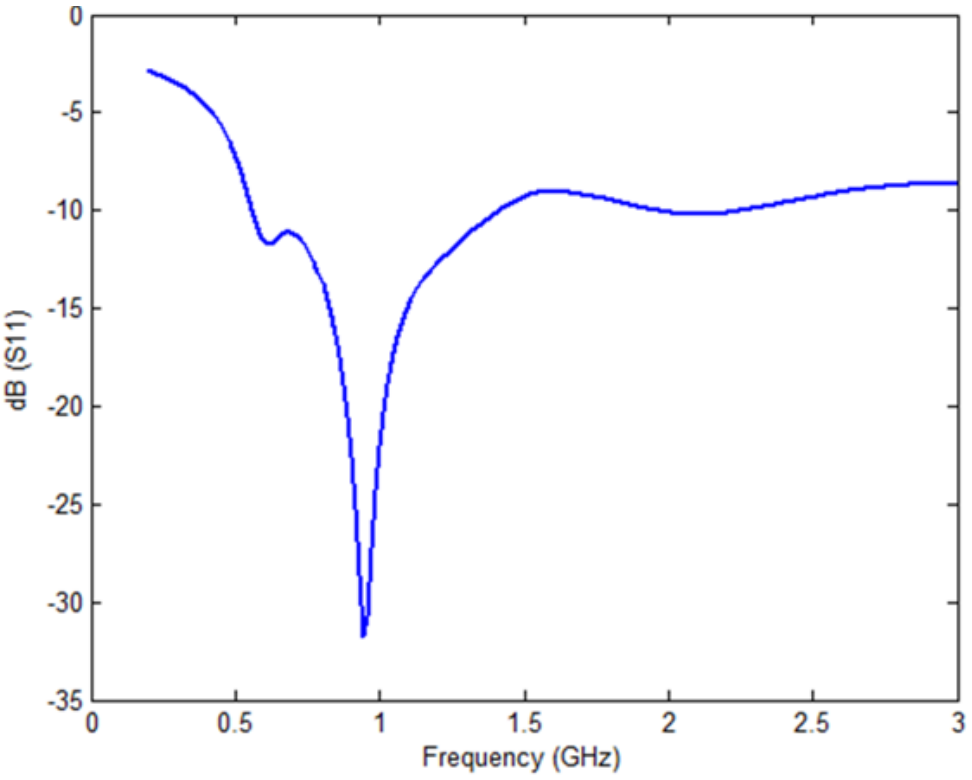

Figure 2.10 915 MHz simulated S11 value

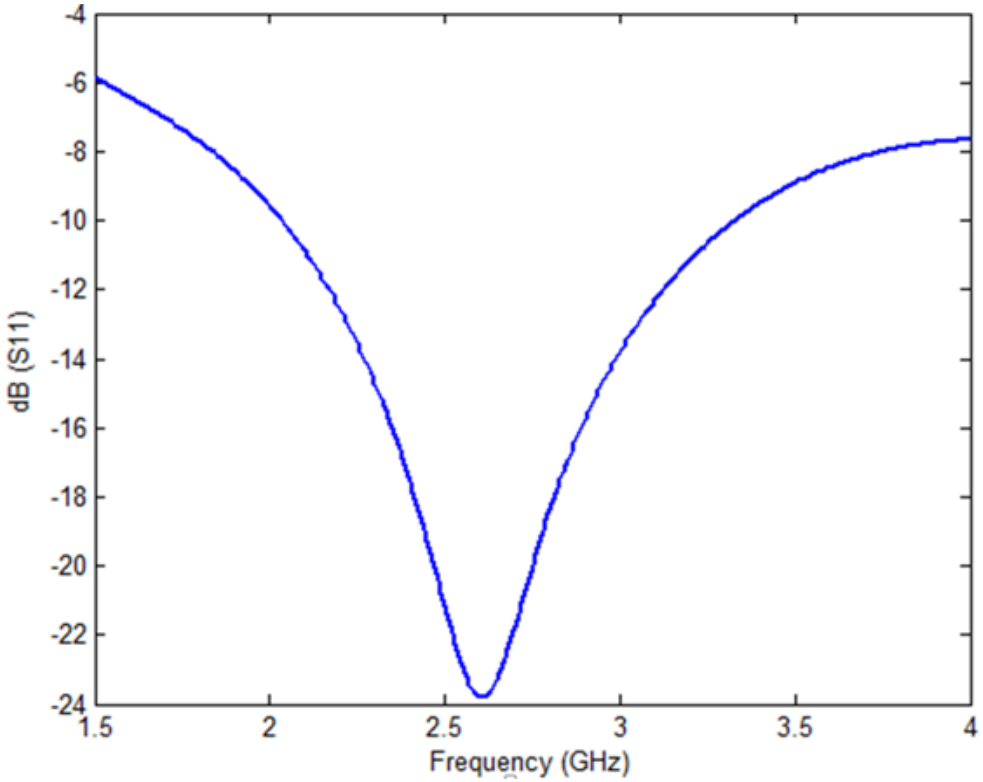

Figure 2.11 2.4 GHz simulated S11 value

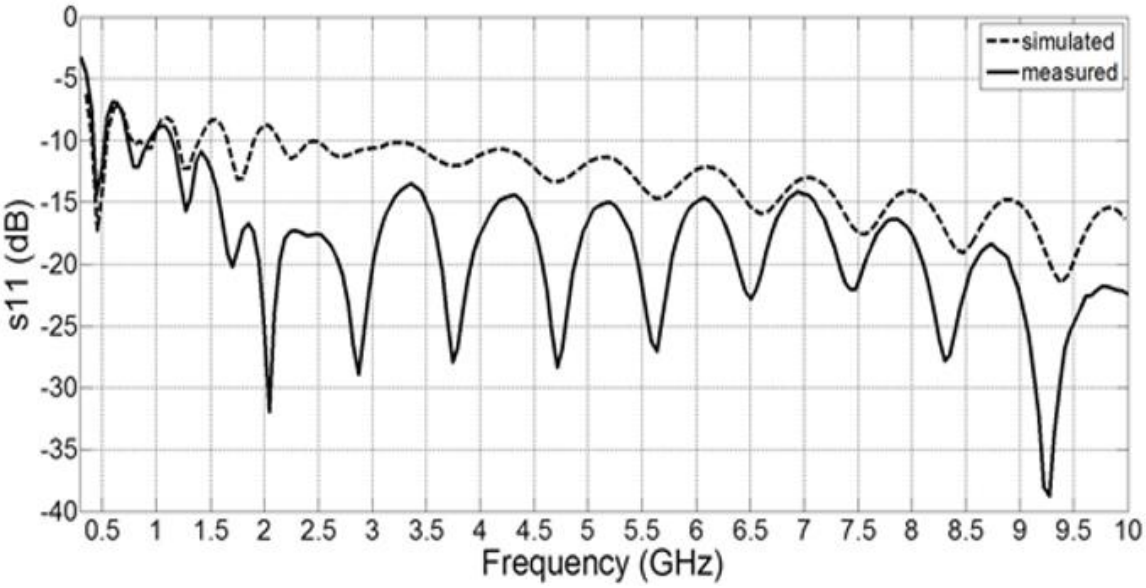

Figure 2.12 Ultra-wideband simulated and measured S11 value

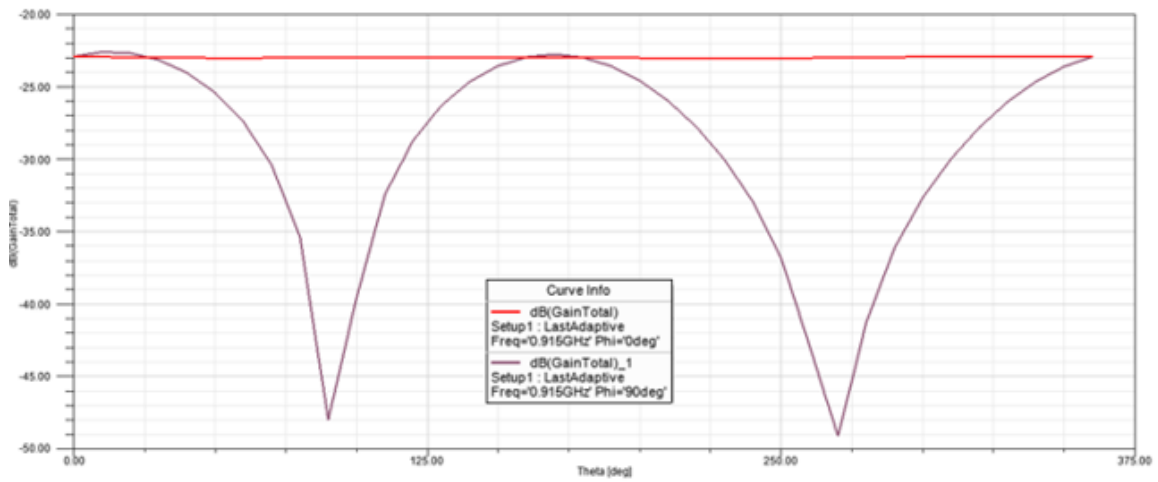

$\varphi = 0, \theta = 0 - 360$

$\varphi = 90, \theta = 0 \ - 360$

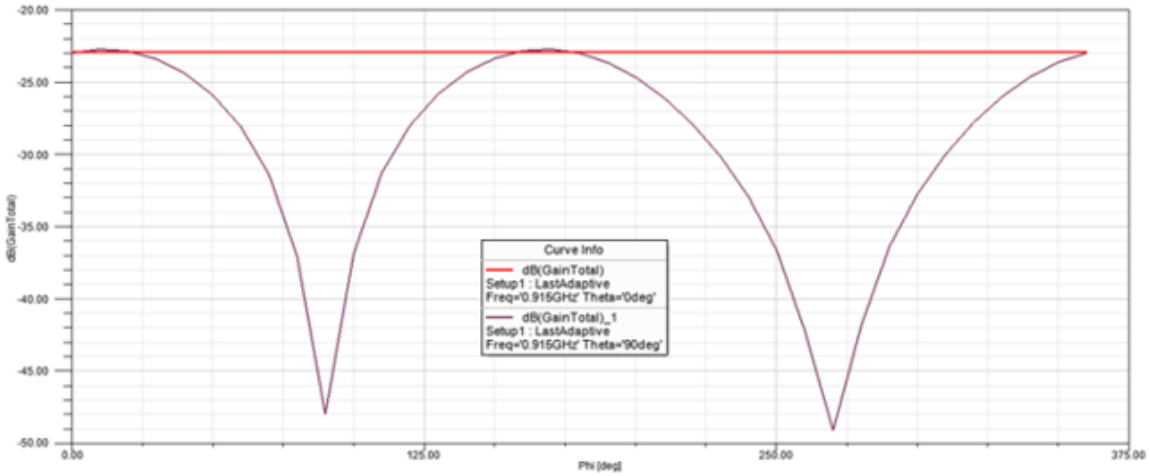

$\theta = 0, \varphi =$ (-180) -180

$\theta = 90, \varphi = (-180) - 180$

Figure 2.13 915 MHz simulated gain pattern

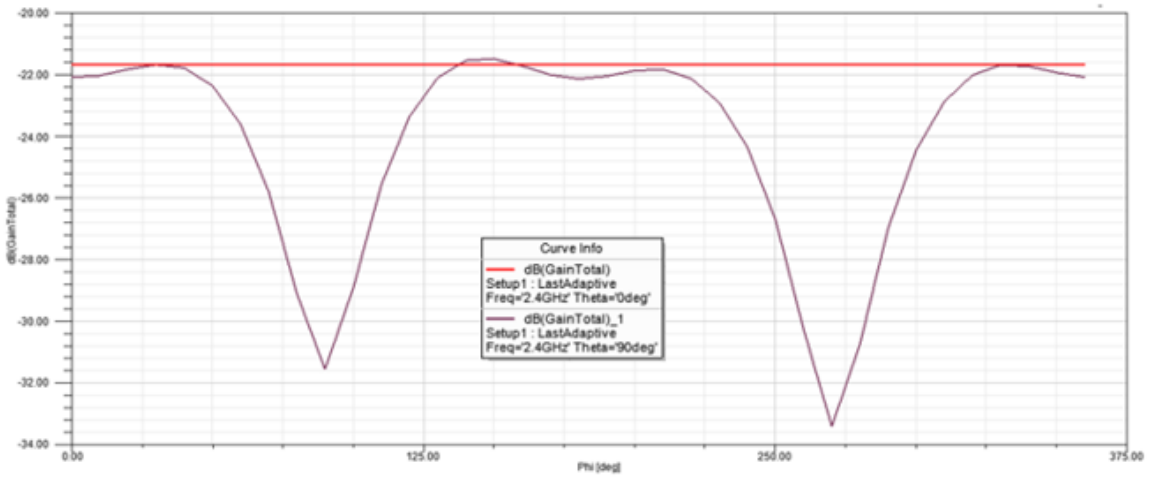

$\varphi = 0, \theta = 0 - 360$

$\varphi = 90, \theta = 0 \ - 360$

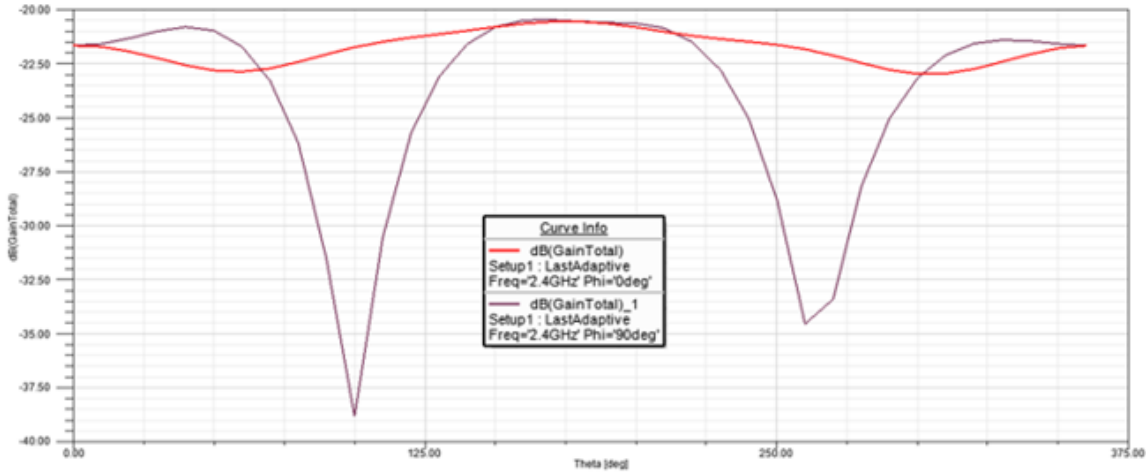

$\theta = 0, \varphi =$ (-180) -180

$\theta = 90, \varphi = (-180) - 180$

Figure 2.14 2.4 GHz simulated gain pattern

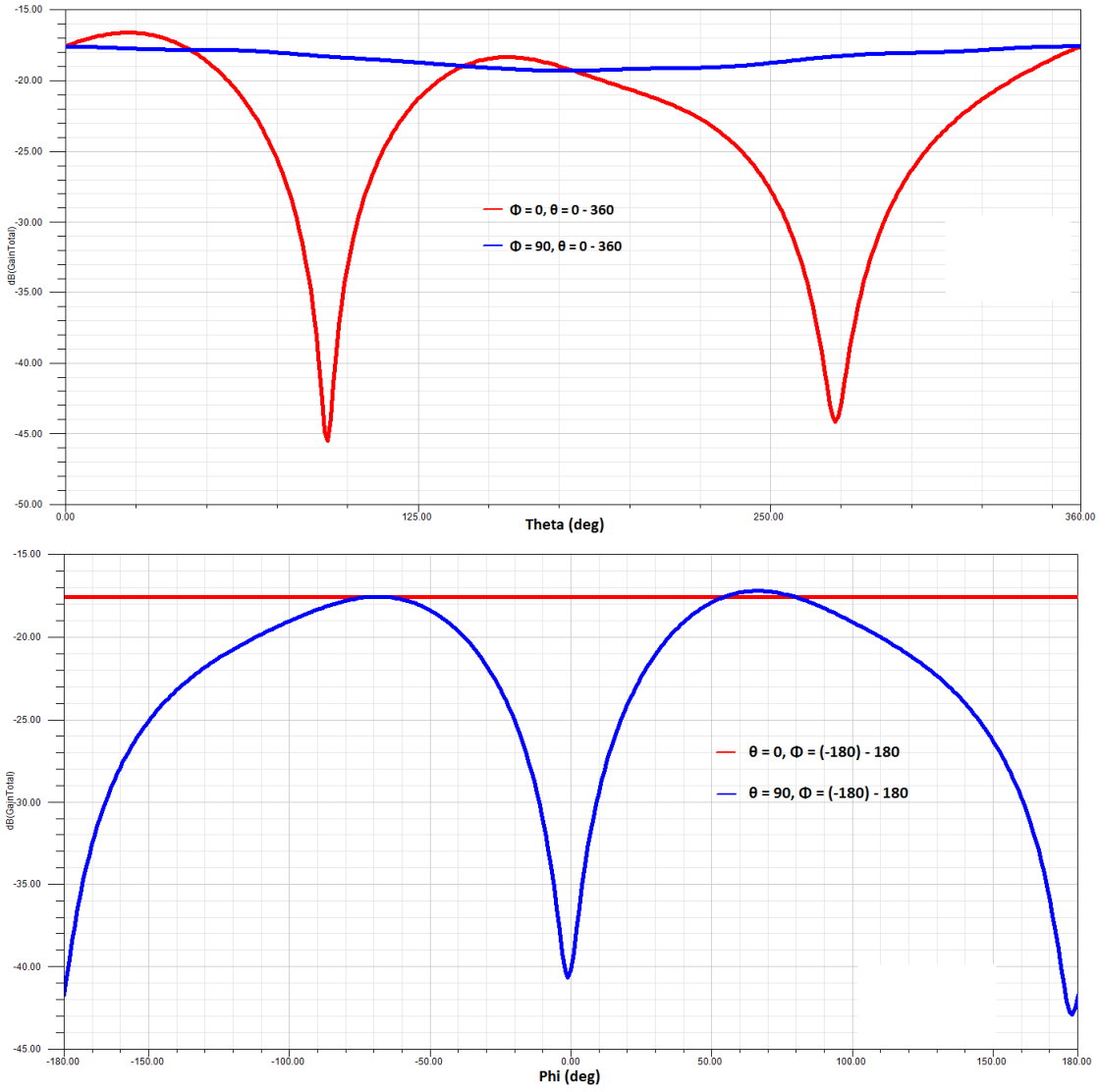

Figure 2.15 Ultra-wideband simulated gain patterns

The specific absorption rate (SAR) is also simulated with the designed antenna applicators and compared to the ultra-wideband applicator shown in Figure 2.16, Figure 2.17, and Figure 2.18 [27]. SAR is described as a measurement of transmitted energy being absorbed by human tissues [34]. SAR results are provided for 915 MHz and 2.4 GHz. These frequencies are regulated by the FCC and fall under the Industrial, Scientific,

and Medical (ISM) band. As the tissue properties change during ablation, the values of the tissue are constantly changing. To simulate this change and observe the differences in SAR, the relative permittivity and conductivity values are changed and shown in Figure 2.19, Figure 2.20, and Figure 2.21 [27].

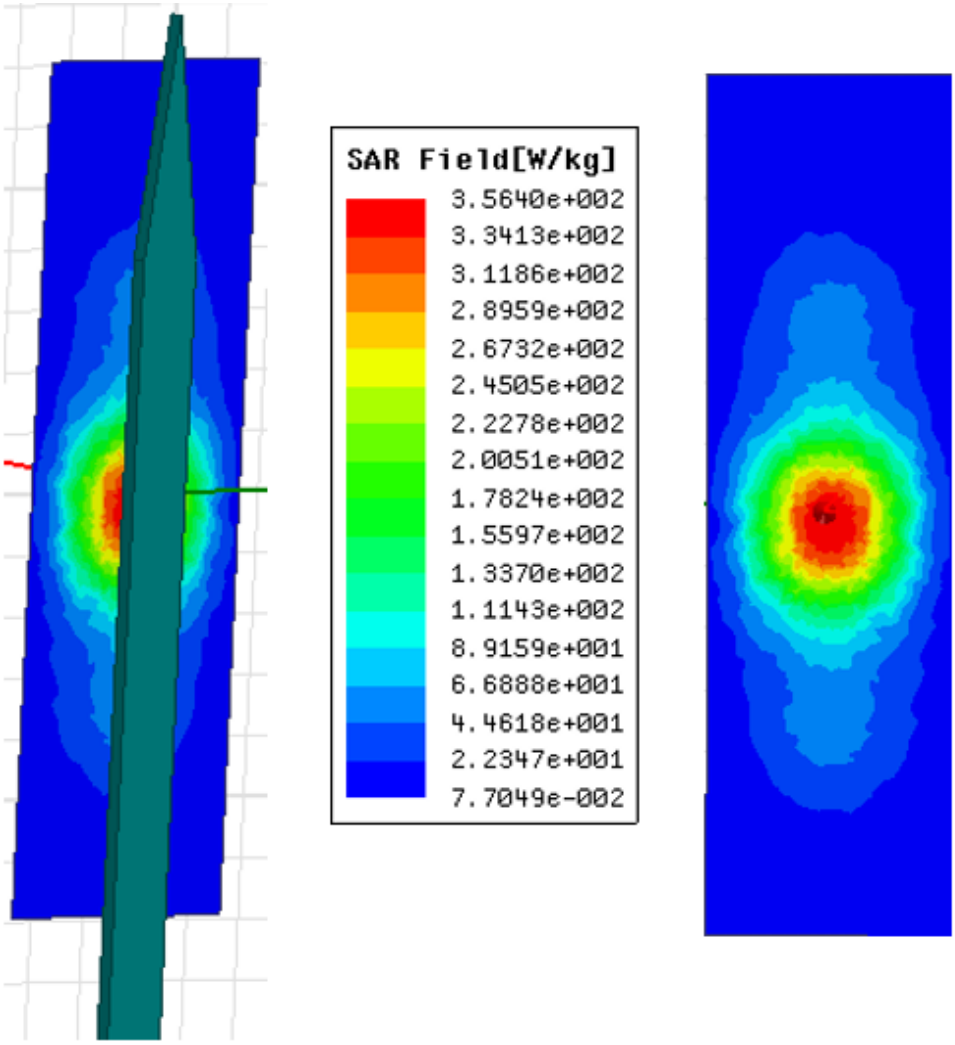

Figure 2.16 915 MHz simulated SAR values

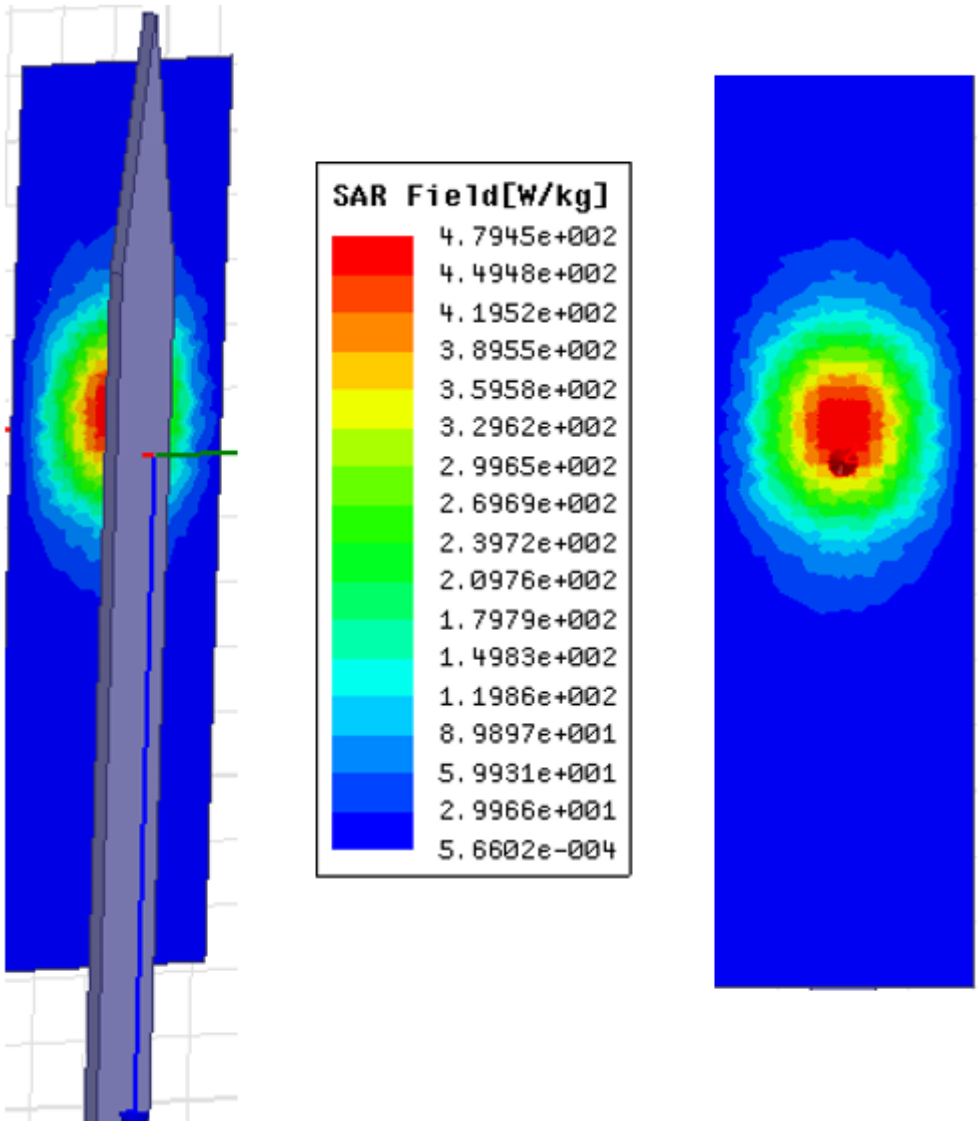

Figure 2.17 2.4 GHz simulated SAR values

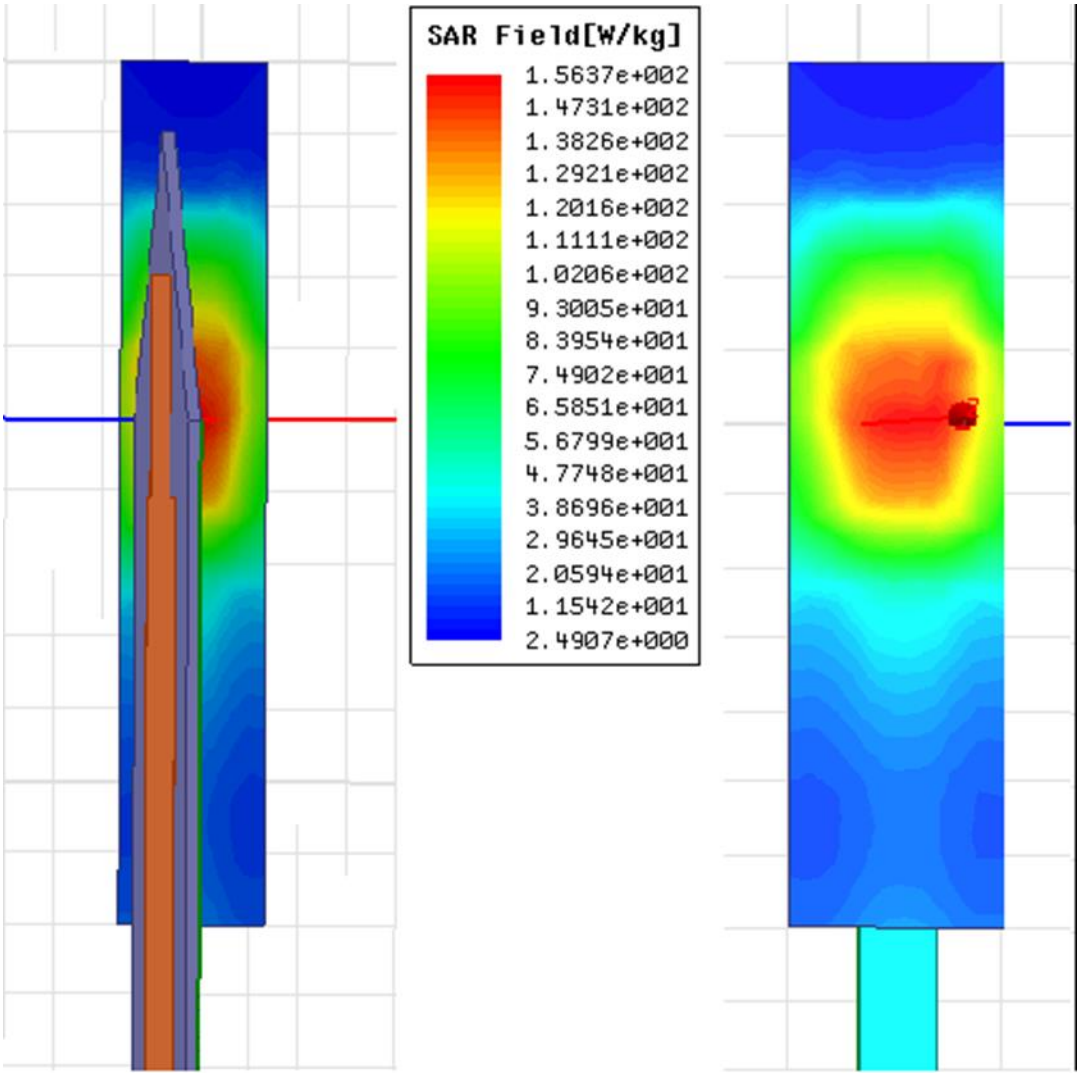

Figure 2.18 Ultra-wideband simulated SAR values at 2.4 GHz

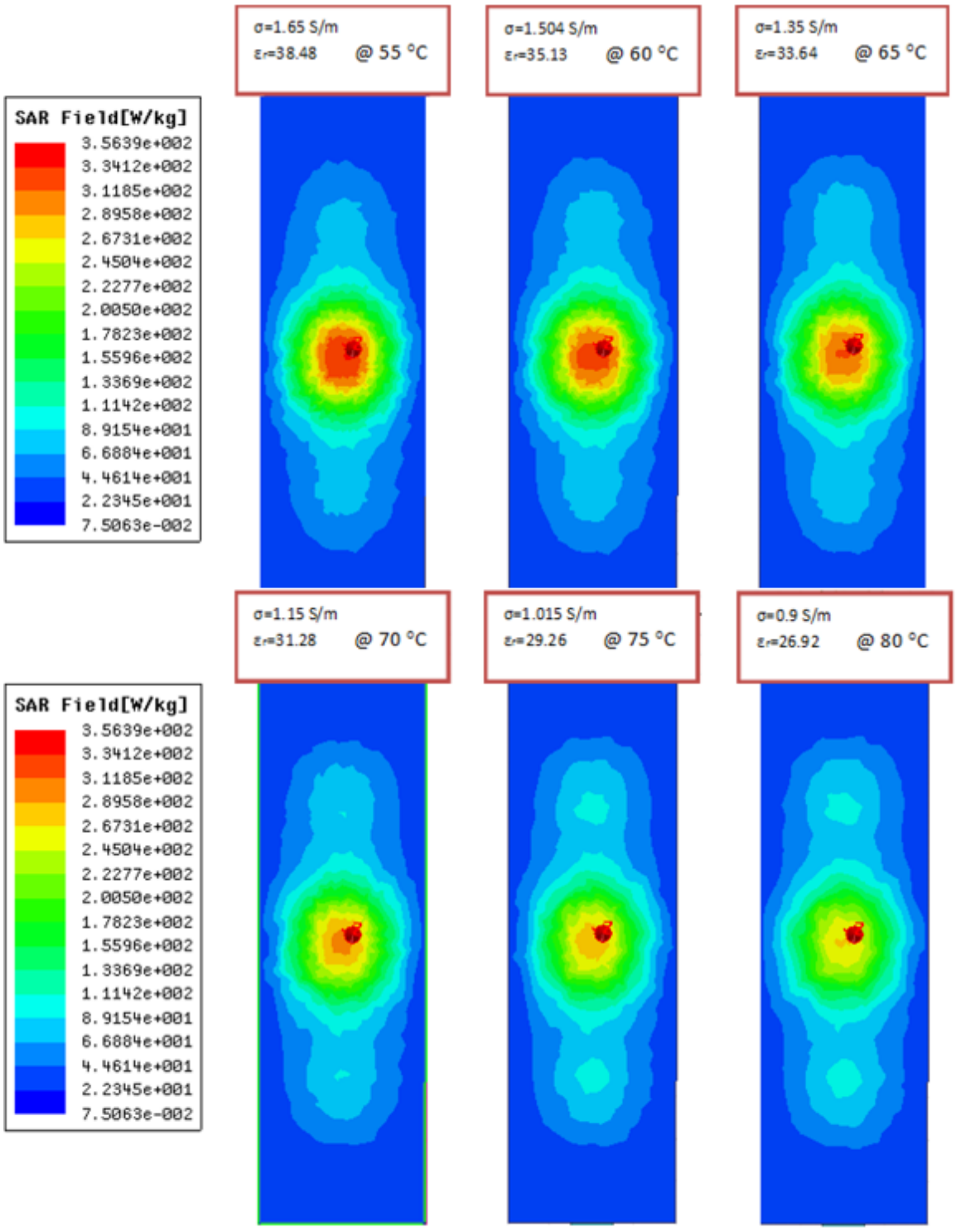

Figure 2.19 915 MHz SAR values as tissue properties change

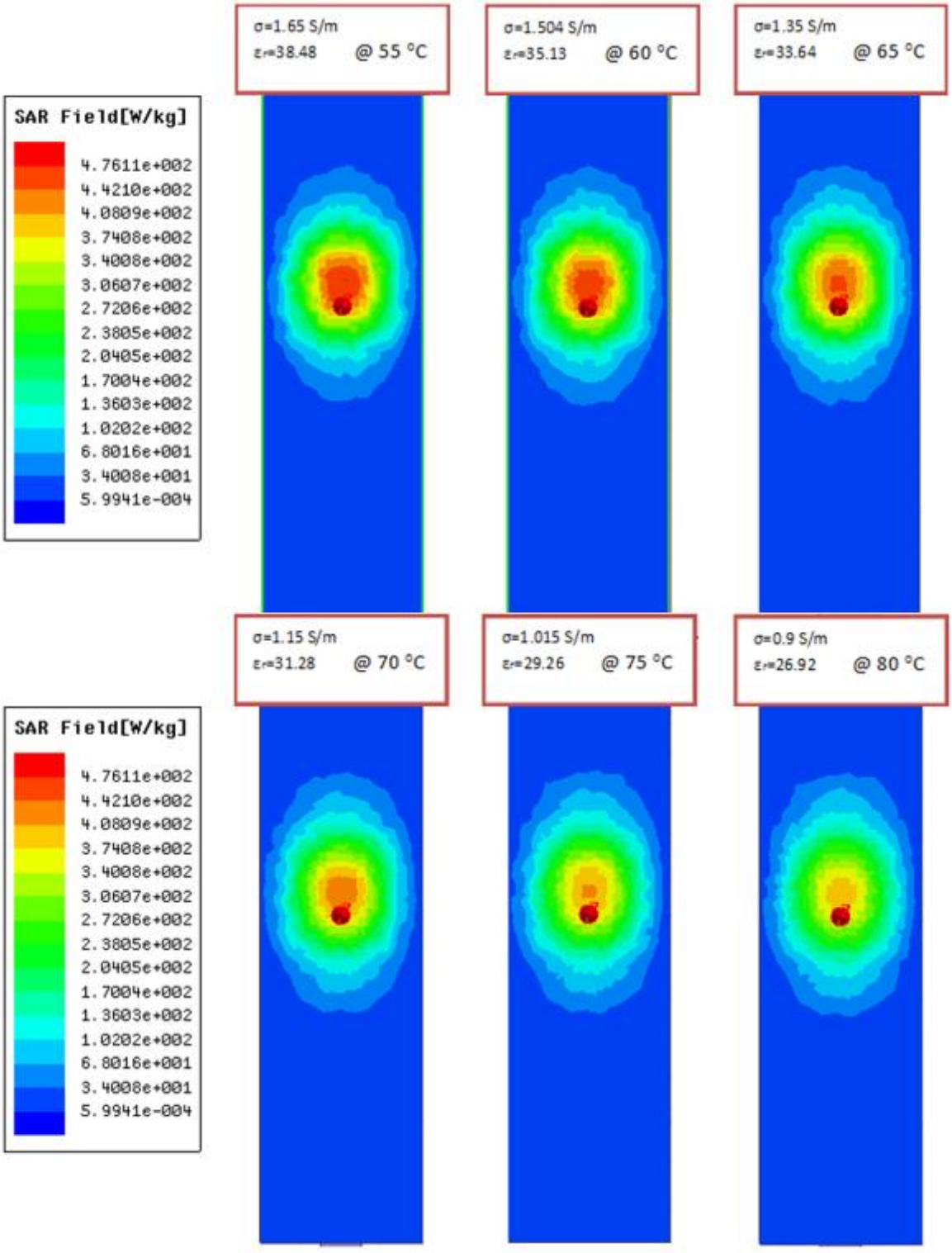

Figure 2.20 2.4 GHz SAR values as tissue properties change

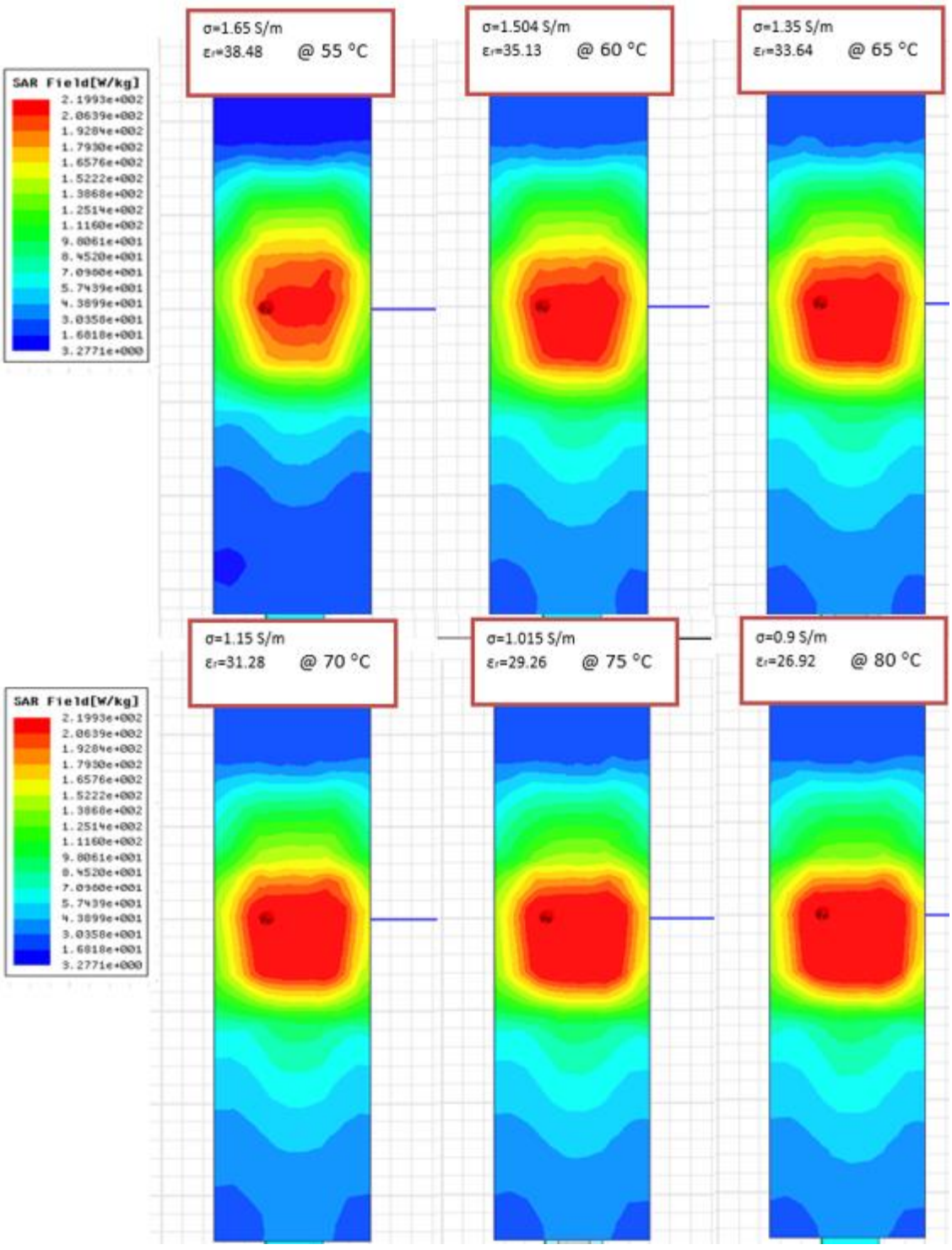

Figure 2.21 Ultra-wideband SAR values at 2.4 GHz as tissue properties change

2.4 Microwave Applicator Fabrication

Once the antennas were designed and simulated, the fabrication process of the applicators were performed. The fabrication was performed in house using the ProtoMat S62 milling machine from LPKF. In order for the milling machine to be used, the design files were first exported from HFSS in a .DXF format. Once this is done, the milling machine communicates with the Circuit CAM 6.1 software to process the design files. To control the rpm of the milling machine the BoardMaster 5.1.210 software would be used to better fabricate on the Rogers R02010 substrate. Fabrication of the antenna applicators is shown in Figure 2.22.

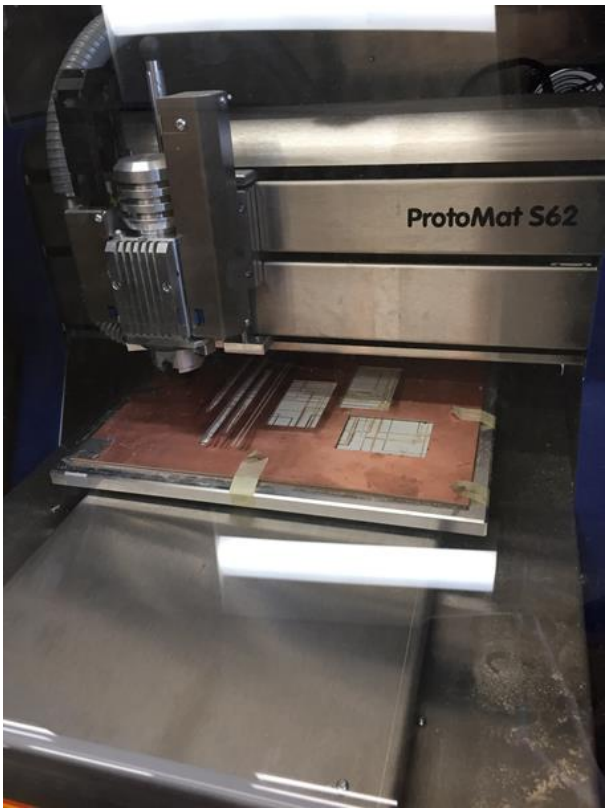

Figure 2.22 Antenna applicator fabrication process

After the fabrication process was completed, the antenna applicators were wrapped with Teflon tape to prevent tail heating and radiation from the feed line and to protect the tip of the applicator from damage while leaving the antenna exposed. The fabricated antennas are shown in Figure 2.23.

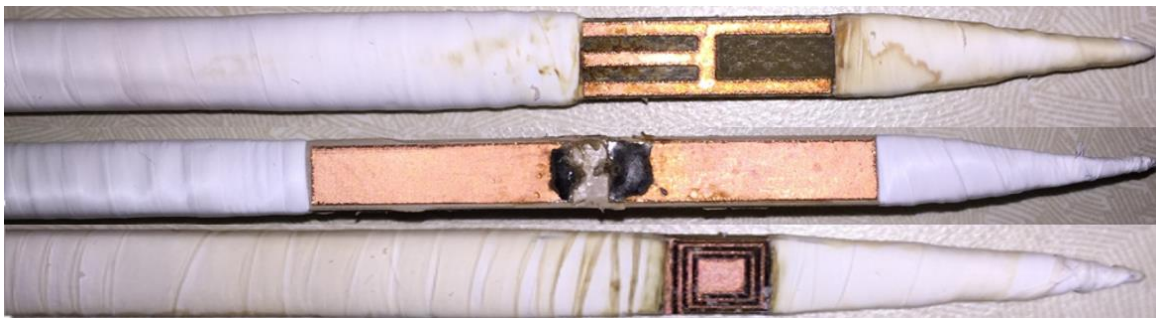

Figure 2.23 Fabricated applicators

CHAPTER III

IN VITRO AND EX VIVO EXPERIMENTS

3.1 In Vivo Dielectric Mimicking Gel Testing

In these experiments, 915 MHz and 2.4 GHz are the two primary frequencies used for testing. In vitro measurements were performed in a liver mimicking gel made from distilled water, vegetable oil, Triton-X 100, gelatin A, salt, ivory soap, and food coloring [38]. The purpose of this experiment is to match the simulated dielectric properties of liver tissue to achieve reliable results before proceeding with ex vivo testing. The comparison of liver to liver gel dielectric properties is shown in Table 3.1 [40]. The fabricated ablation antenna applicator is encased in liver mimicking gel and is shown in Figure 3.2. The measured S11 values are then obtained for each antenna and shown in Figure 3.3, Figure 3.4, and Figure 3.5.

Time (min)	MW power	Temperature (°C)		Relative permittivity (ε_r)		Conductivity (σ, S m^{-1})	
		Mean	U(95%)	Mean	U(95%)	Mean	U(95%)
0	ON	15.0	4.46%	44.98	2.01%	1.79	5.18%
1	ON	48.1	3.57%	43.43	3.36%	1.71	6.14%
2	ON	74.7	4.99%	40.65	6.46%	1.66	6.22%
3	ON	82.3	4.01%	39.22	5.76%	1.63	5.65%
4	ON	89.7	2.64%	37.66	6.42%	1.59	5.69%
5	ON	93.3	2.14%	35.26	6.07%	1.55	5.79%
6	ON	95.4	1.92%	32.12	6.58%	1.43	6.05%
7	ON	96.8	1.18%	30.47	7.19%	1.38	6.46%
8	ON	97.8	0.82%	29.04	7.49%	1.34	7.17%
9	ON	98.2	0.72%	27.61	6.58%	1.30	6.37%
10	ON	98.9	0.56%	26.76	7.13%	1.26	7.86%
12	OFF	75.2	2.43%	26.11	7.13%	1.20	8.25%
14	OFF	55.8	6.53%	26.50	7.08%	1.19	8.53%
16	OFF	48.6	6.53%	27.00	7.13%	1.19	8.54%
18	OFF	43.2	6.51%	27.60	7.19%	1.19	8.55%
20	OFF	39.6	6.56%	28.00	7.46%	1.20	9.02%

Figure 3.1 Liver properties vs temperature

Figure 3.2 Ultra-wideband applicator encased in liver mimicking gel

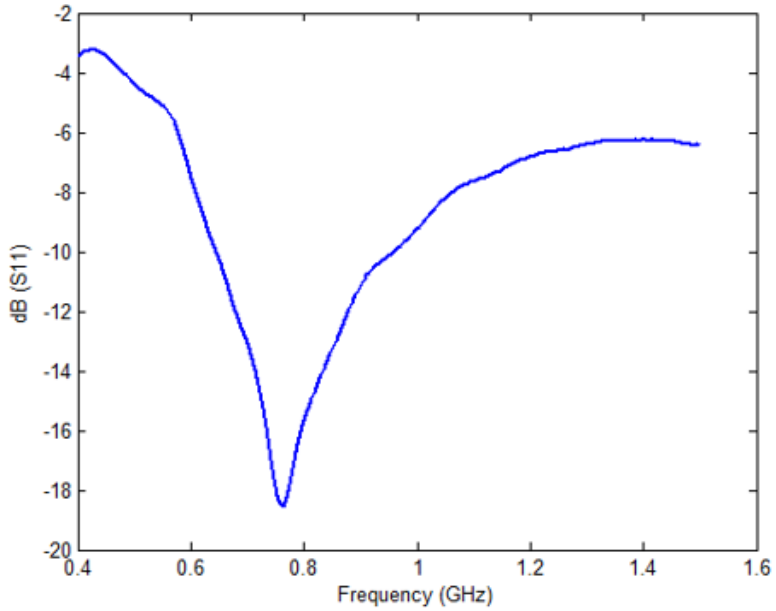

Figure 3.3 915 MHz applicator S11 gel measurements

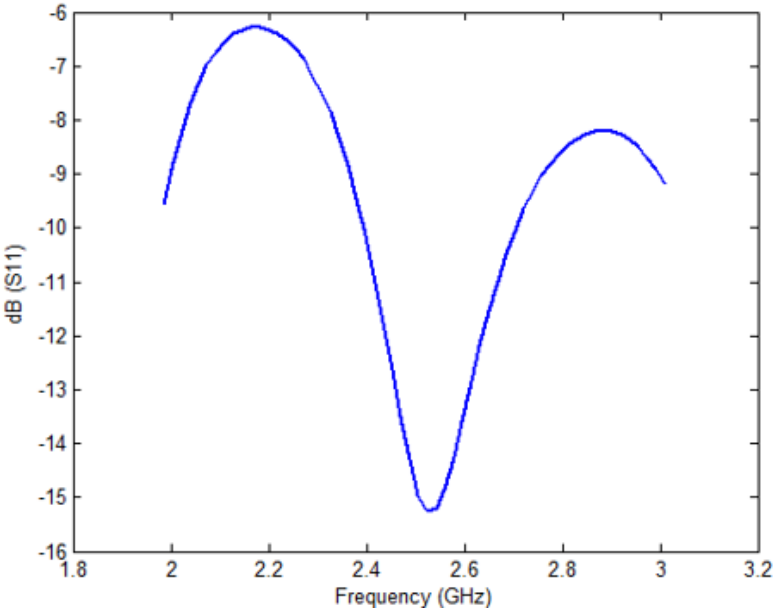

Figure 3.4 2.4 GHz applicator S11 gel measurement

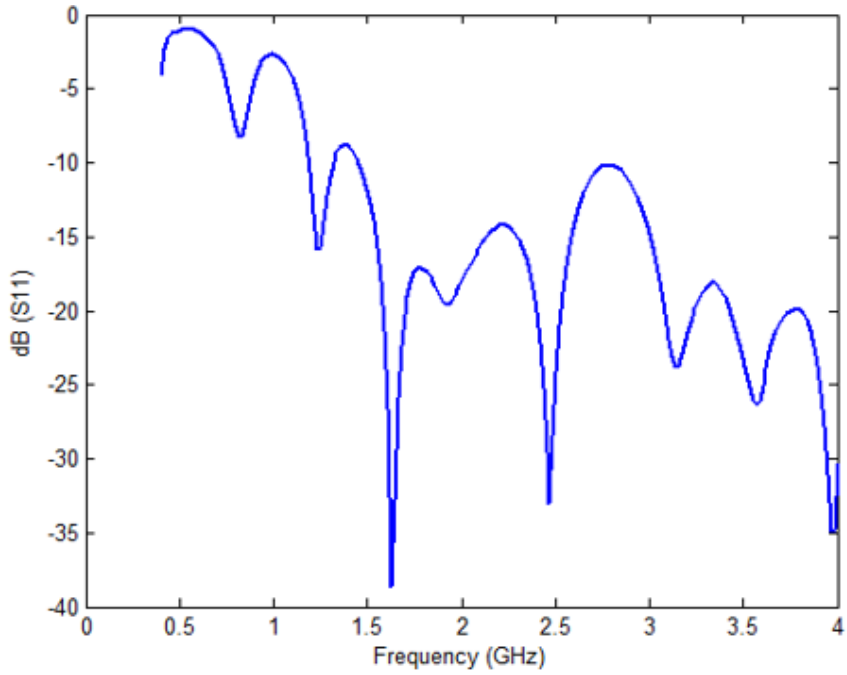

Figure 3.5 Ultra-wideband applicator S11 gel measurement at 2.4 GHz

3.2 Ex Vivo Porcine Liver Testing

The In Vivo gel testing showed promising results in terms of return loss, which allowed the study to progress to Ex Vivo porcine liver testing. The setup required to perform Ex Vivo tests included a power amplifier, signal generator, network analyzer, fiber optic temperature sensor, coaxial cables, adapters, ablation applicators, and porcine liver. The full experiment setup can be seen in Figure 3.6. Once the setup was finalized, S11 measurements were taken with each applicator in an unaltered porcine liver. The resulting measurements are shown in Figure 3.7, Figure 3.8, and Figure 3.9.

Figure 3.6 Experiment setup

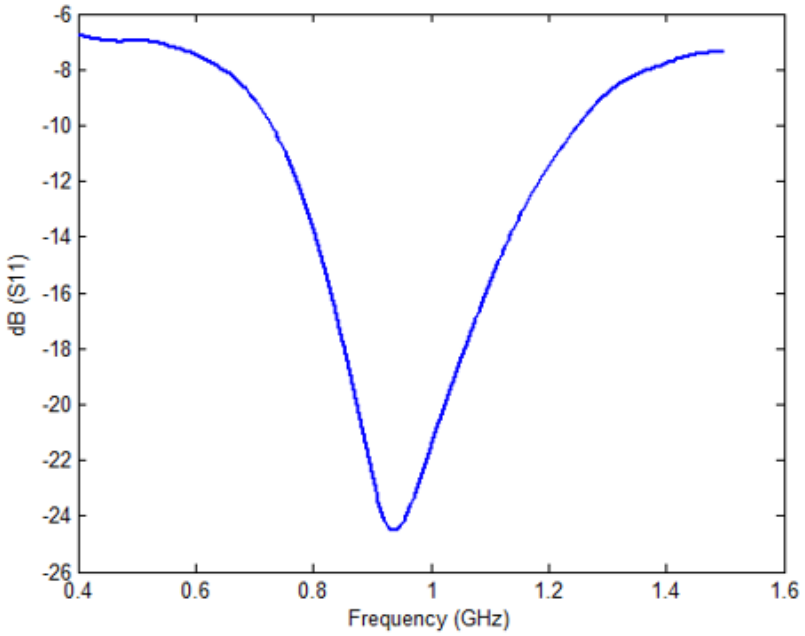

Figure 3.7 915 MHz NB applicator S11 in porcine liver

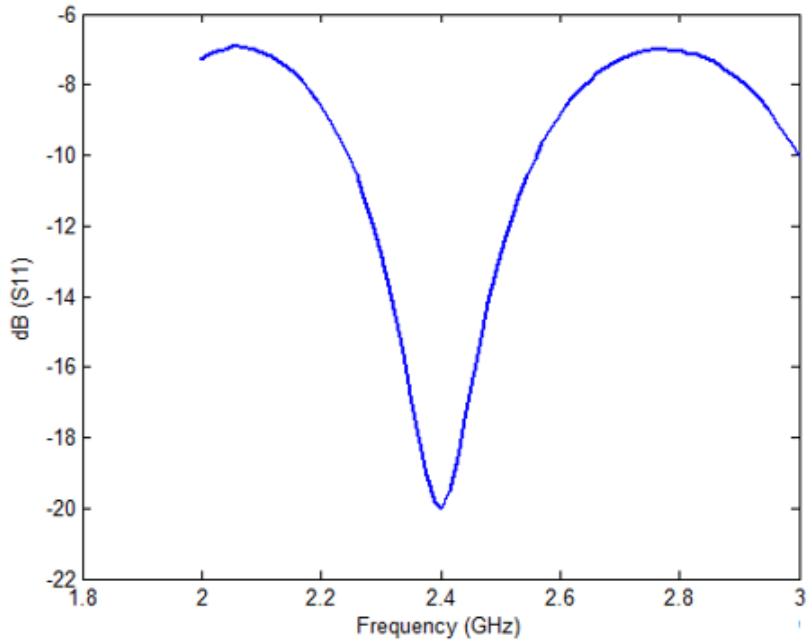

Figure 3.8 2.4 GHz NB applicator S11 in porcine liver

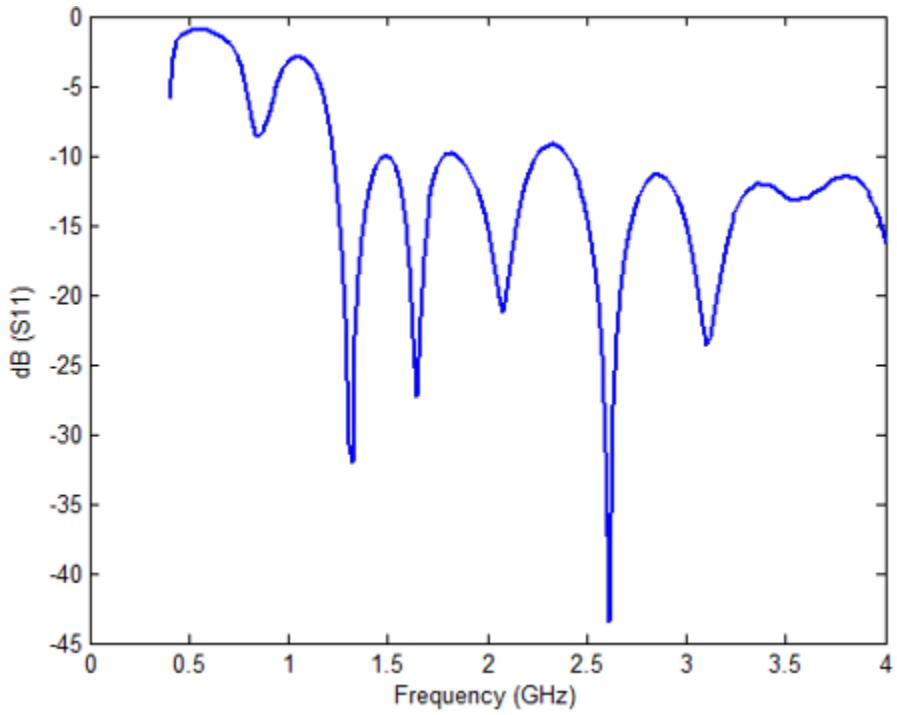

Figure 3.9 2.4 GHz UWB applicator S11 in porcine liver

In the experiment setup, a power amplifier is connected to an Agilent MXG analog signal generator. The signal generator is used to send the signal through the power amplifier, which is connected to the MW applicators. The power amplifier used for the 915 MHz antenna is the Amplifier Research 5W1000 while the 2.4 GHz antennas required a Hughes Traveling Wave Tube Amplifier 1177H. Each antenna applicator is placed inside of the porcine liver and then the tissue is exposed to 5W of power at 915 MHz and 2.4 GHz for time periods of 5 and 10 minutes. The ablation results for each antenna applicator at (left) 5 min ablation and (right) 10 minute ablation is shown in Figure 3.10, Figure 3.11, and Figure 3.12 respectively. After the ablation testing was complete with each applicator, the S11 is measured using an Agilent PNA network analyzer E8362B to compare with simulated results. The S11 values are shown for each

applicator with (left) 5 minute ablation and (right) 10 minute ablation in Figure 3.13, Figure 3.14, and Figure 3.15.

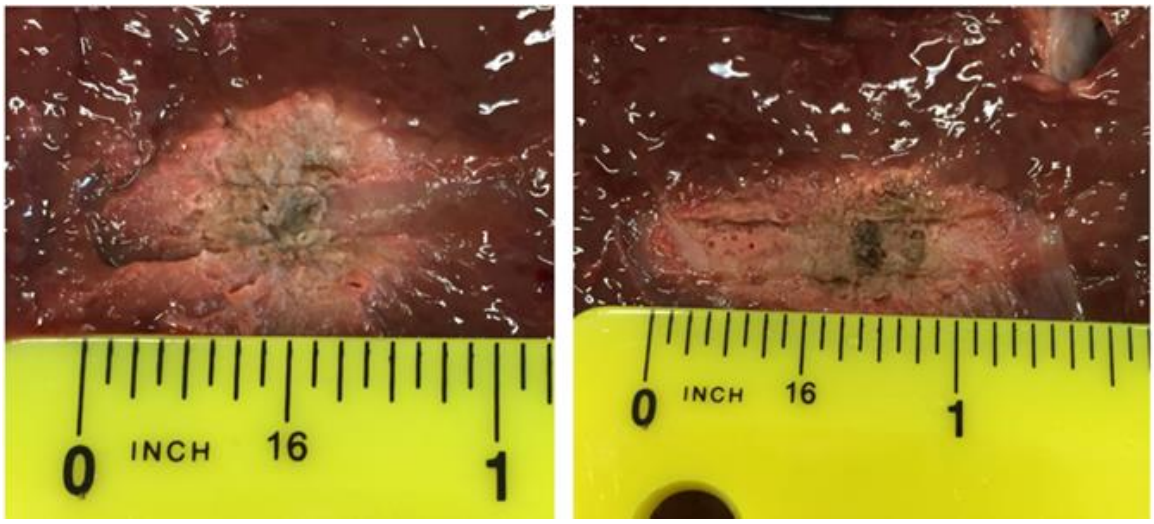

Figure 3.10 915 MHz NB ablation zone

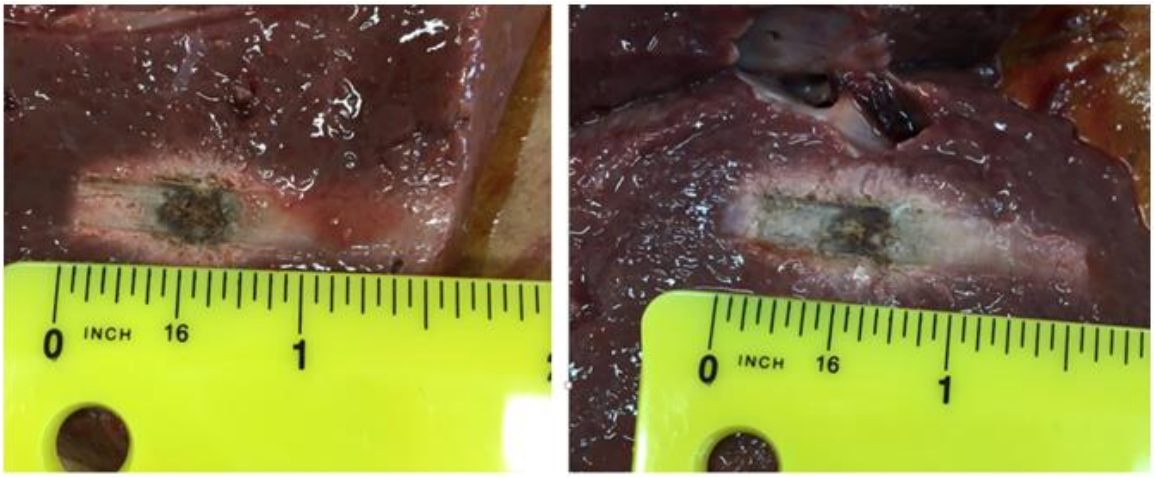

Figure 3.11 2.4 GHz NB ablation zone

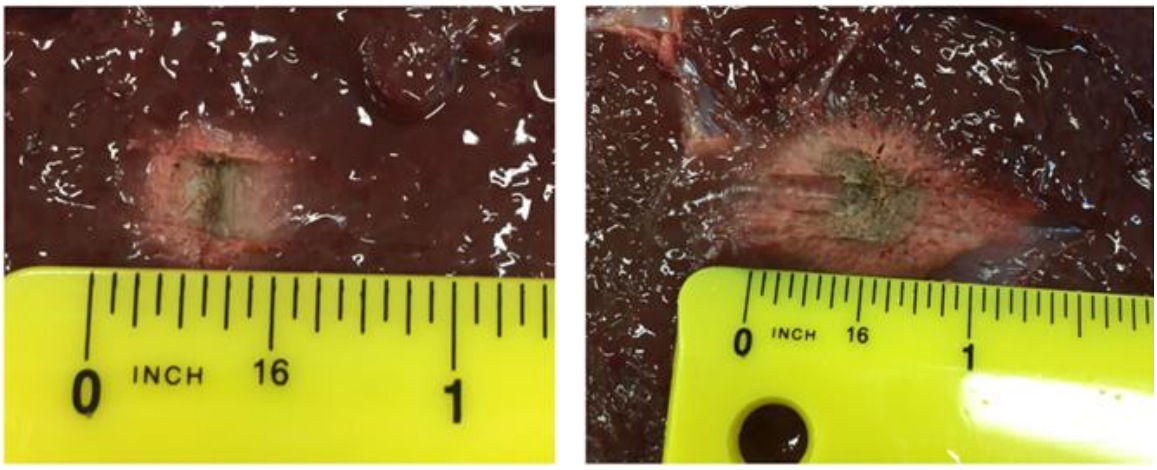

Figure 3.12 2.4 GHz UWB ablation zone

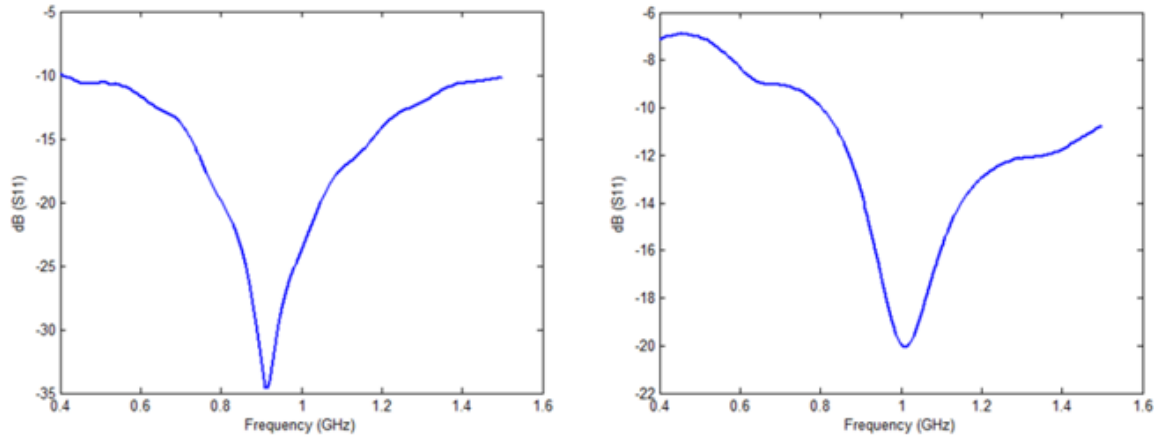

Figure 3.13 915 MHz NB S11

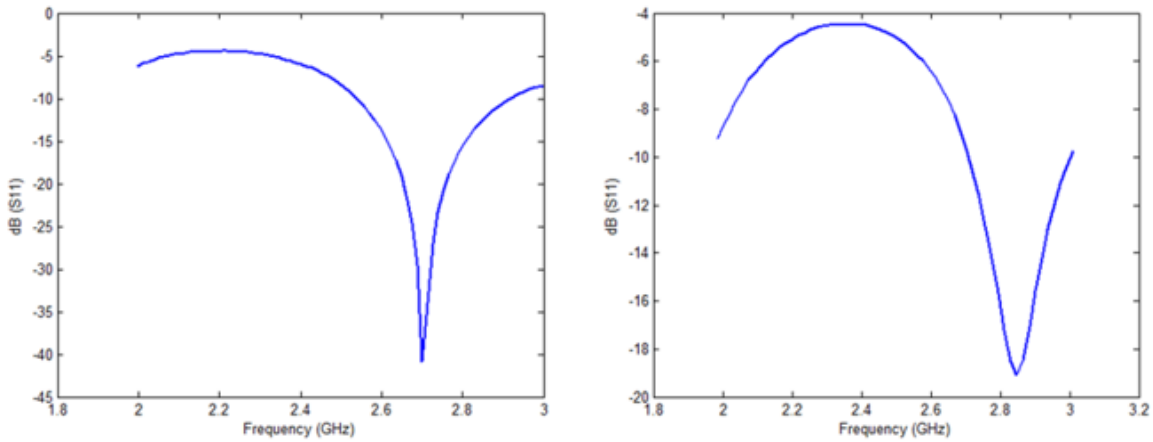

Figure 3.14 2.4 GHz NB S11

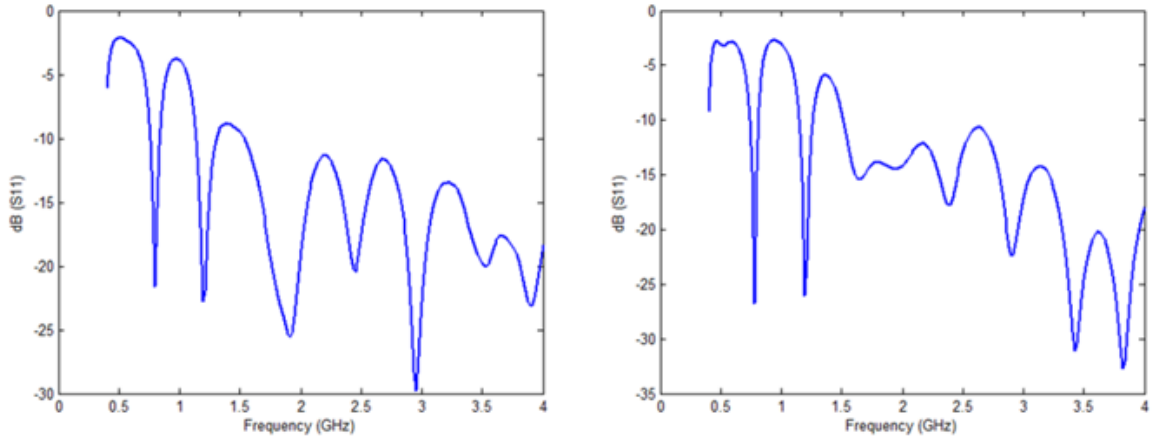

Figure 3.15 2.4 GHz UWB S11

These results show that the narrowband applicators reflection coefficient is shifting due to the tissue properties changing as heating occurs, which leaves an undesirable amount of ablation. As the tissue begins to lose water content during the heating process, the relative permittivity and conductivity of the tissue begin to drop [39]. These changes affect the impedance matching of the antenna applicator, which results in a significant loss in power transmission efficiency. The change in tissue properties as

temperature increases is shown in Figure 3.16, and Figure 3.17 [40]. As the power reflection increases, in order to get a desired ablation zone, more power and longer ablation times are required. In actual studies, multiple narrowband ablation applicators are used at different resonating frequencies to prevent these undesired ablation zones.

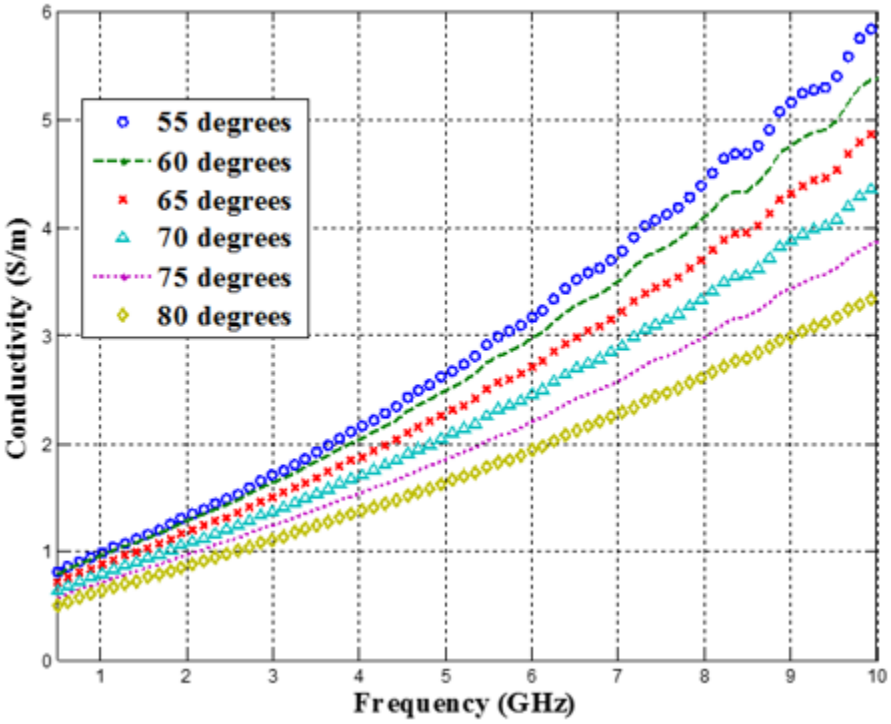

Figure 3.16 Effect of temperature increase on conductivity in porcine liver

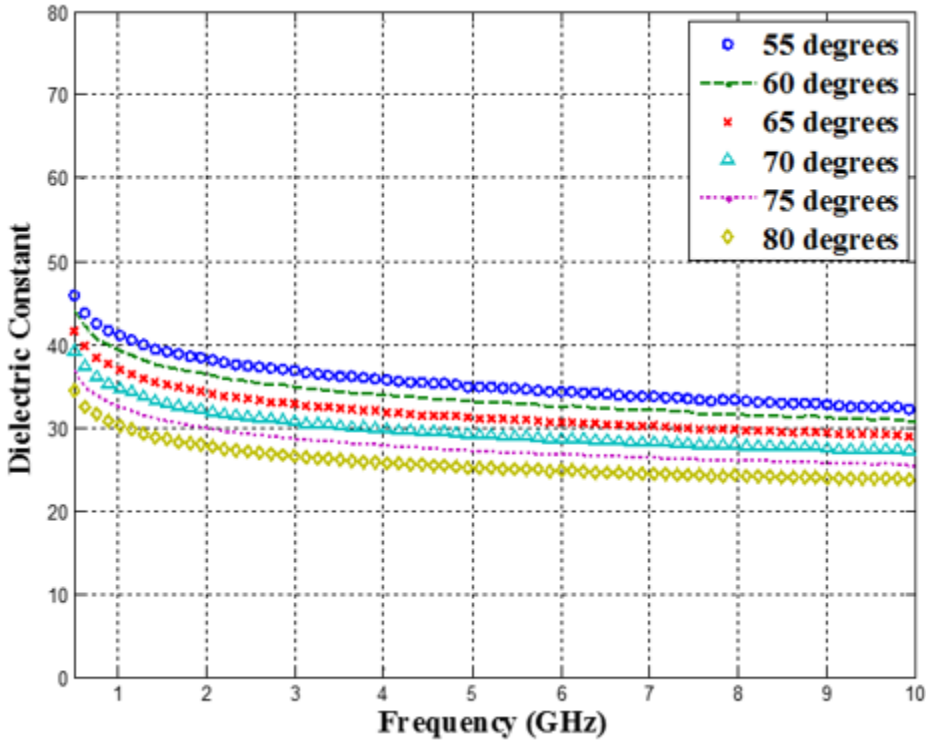

Figure 3.17 Effect of temperature increase on relative permittivity in porcine liver

The measurements from the ultra-wideband antenna suggest that, even at a lower power, a desirable ablation zone is achieved. Increasing the ablation zone could be achieved by increasing the frequency or amount of supplied power. Though the bandwidth of the ultra-wideband applicator changed, the resonating frequency maintained efficient. The benefit of this MW applicator is that the power transmission efficiency can maintain between 95% and 99.9% in the frequency range of 300 MHz to 10 GHz shown in Figure 3.18 [27].

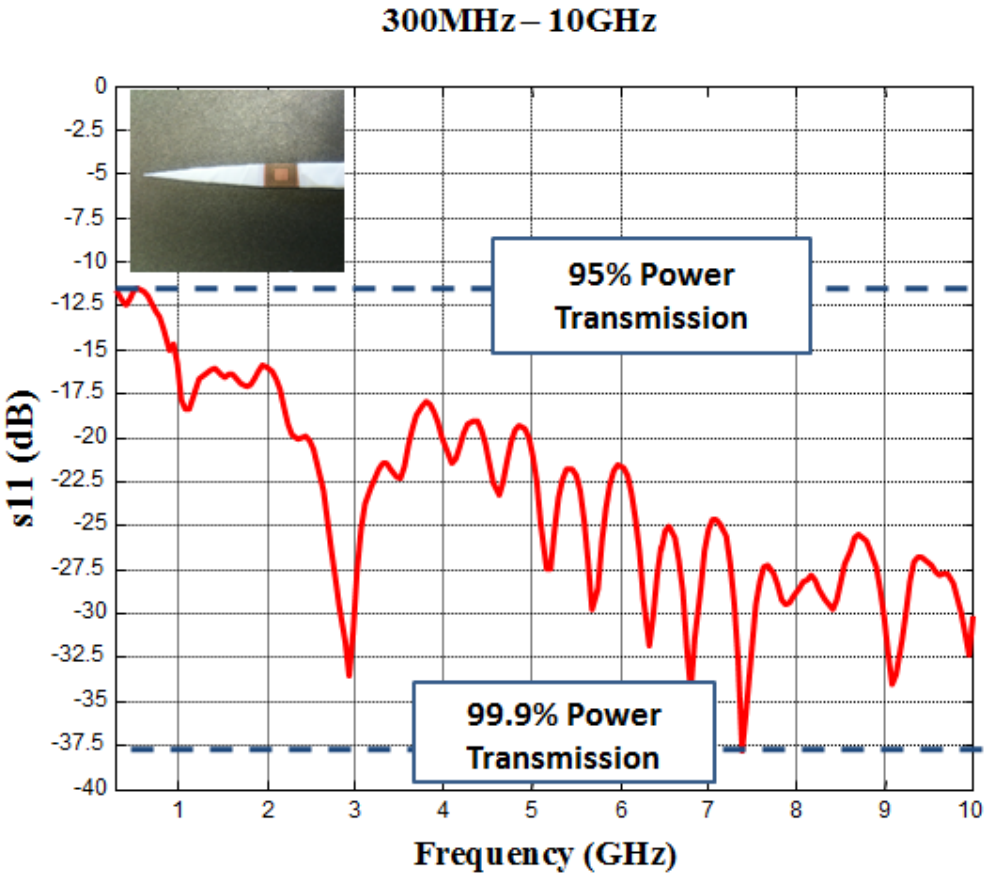

Figure 3.18 Power transmission efficiency of UWB applicator

CHAPTER IV

CONCLUSION AND FUTURE WORK

In conclusion, two narrowband microwave ablation applicators are designed, simulated, and tested. The study compares the results of these applicators to an ultra-wideband microwave ablation applicator. These tests show that many narrowband ablation systems can cause undesirable ablation zones in comparison to ultra-wideband systems. Also, during the experiments, it is shown that ultra-wideband ablation systems are able to create a desirable ablation zone at lower frequency ranges with a low amount of power.

As a future work, these applicators should be designed, fabricated, and tested on a cylindrical probe. Testing multiple narrowband applicators for creating one ablation zone with less undesirable zones would also be beneficial to compare to ultra-wideband systems.

REFERENCES

[1] W. L. Clark, J. D. Morgan, and E. J. Asnis, "Electrothermic methods in the treatment of neoplasms and other lesions, with clinical and histological observations," *Radiology*, vol.2, pp. 233-246, 1924.

[2] J. P. McGahan and V. A. Raalte, "History of Ablation – Section 1," in *Tumor Ablation Principles and Practice,* 1st ed. Springer New York, 2005, pp. 3-16.

[3] I. D. McRury and D. E. Haines, "Ablation for the treatment of arrhythmias," *Proc. IEEE,* vol.84, no.3, March 1996.

[4] K. K. Ng et al., "Thermal ablative therapy for malignant liver tumors: a critical appraisal," J Gastroenterol Hepatol, vol.18, pp. 616-629, June 2003.

[5] B. Rubinsky, "Cryosurgery," Annu Rev Biomed Eng., vol. 2, pp. 157- 187, Aug. 2000.

[6] R. W. Habash, R. Bansal, D. Krewski, and H. T. Alhafid, "Thermal therapy, part iii: ablation techniques," Crit. Rev. Biomed. Eng., vol. 35, pp. 37-121, 2007.

[7] Y. F. Zhou, "High intensity focused ultrasound in clinical tumor ablation," *World J. Clin. Oncol,* 2011.

[8] D. E. Haines, "Thermal ablation of perfused porcine left ventricle in vitro with the neodymium-YAG laser hot tip catheter system," Pacing Clin. Electrophysiol, vol.15, pp. 979-985, Aug. 1992.

[9] T. L. Wonnell, P. R. Satuffer, and J. J. Langberg, "Evaluation of microwave and radio frequency catheter in myocardium-equivalent phantom model," *IEEE Trans. Biomed. Eng.,* vol.39, no.10, Oct. 1992.

[10] M. Friedman et al., "Radiofrequency ablation of cancer," J. Cardiovasc Intervent Radiol, vol.27, pp. 427-434, June 2004.

[11] S. Pisa, M. Cavagnaro, P. Bernardi, and J. C Lin, "A 915-MHz antenna for microwave thermal ablation treatment: physical design, computer modeling and experimental measurement," IEEE Trans. Biomed. Eng., vol. 48, no. 5, pp., 599601, May 2001.

[12] E. S. Glazer and S. A. Curley, “the ongoing history of thermal therapy for cancer,” Surg. Oncol. Clin. N. Am., vol. 20, pp. 229-235, Apr. 2011.

[13] C. L. Brace, “Radiofrequency and microwave ablation of the liver, lung, kidney and bone: what are the differences?” Curr. Probl. Diagn. Radiol, vol.38, pp. 135143, May 2009.

[14] M. R. Williams, M. Garrido, M. C. Oz, and M. Argenziano, “Alternative energy sources for surgical atrial ablation,” J Card. Surg., vol. 19, pp. 201-206, May 2004.

[15] Y. Minami and M. Kudo, “Radiofrequency ablation of hepatocellular carcinoma: a literature review,” Int. J. Hepatol, vol. 2011, pp. 1-9, Feb. 2011.

[16] Y. K. Cho, J. K. Kim, W. T. Kim, and J. W. Chung, “Hepatic resection versus radiofrequency ablation for very early stage hepatocellular carcinoma: a markov model analysis,” Hepatology, vol. 51, no. 4, pp. 1284–1290, Apr. 2010.

[17] J. Langberg et al., “Catheter ablation of accessory pathways using radiofrequency energy in the canine coronary sinus,” J. Am. Coll. Cardiol., vol.13, pp. 491-496, Feb. 1989.

[18] L. T. Blouin and F. I. Marcus, “The effect of electrode design on the efficiency of delivery of radiofrequency energy to cardiac tissue in vitro,” Pacing Clin. Electrophysiol, vol.12, pp. 136-143, Jan. 1989.

[19] F. H. Wittkampf, R. N. Hauer, and E. O. Robles de Medina, “Control of radiofrequency lesion size by power regulation,” Circulation, vol.80, pp. 962-968, Oct. 1989.

[20] A. Goette, S. Reek, H. U. Klein, and J. C. Geller, “Case report: severe skin burn at the site of the indifferent electrode after radiofrequency catheter ablation of typical atrial flutter,” J. Interv. Card. Electrophysiol, vol.5, pp. 337-340, Sep. 2001.

[21] D. A. Iannitti, R. C. G. Martin, C. J. Simon, W. W. Hope, W. L. Newcomb, K. M. McMasters, and D. Dupuy, “Hepatic tumor ablation with clustered microwave antennae: the US phase II Trial,” *HPB*, vol.9, pp. 120-124, 2007.

[22] “Tumor Ablation,” Thermal Ablation Research Lab. 2014. [Online] Available http://www.academicdepartments.musc.edu/ablation

[23] “Leading Solutions for Thermal Ablation,” 2015. [Online] Available http://www.covidien.com/surgical/products/ablation-systems

[24] D. M. Lloyd et al., "International multicenter prospective study on microwave ablation of liver tumours: preliminary results," HPB (Oxford), vol.13, pp. 579585, Aug. 2011.

[25] T. Zerner, "The physics of Microwave Ovens," Year 12 Physics Information Search Presentation, 2010. [Online] Available http://tobyzerner.com/microwaves

[26] D. Yang, M. C. Converse, D. M Mahvi, and J. G. Webster, "Measurement and analysis of tissue temperature during microwave liver ablation," IEEE Trans. Biomed. Eng., vol. 54, pp. 150-155, Jan. 2007.

[27] M. Asili, "Ultra-wideband microwave ablation applicators," Mississippi State University, 2014. [Online] Available http://gradworks.umi.com/15/54/1554886

[28] D. M. Lloyd et al., "International multicenter prospective study on microwave ablation of liver tumours: preliminary results," HPB (Oxford), vol.13, pp. 579585, Aug. 2011.

[29] C. J. Simon, D. E. Dupuy, and W. W. Mayo-smith, "Microwave ablation: principles and applications," *RadioGraphics,* pp. 69-83, Oct. 2005.

[30] "IEEE standard definitions of terms for antennas," [online]. Available: http://ieeexplore.ieee.org/stamp/stamp.jsp?tp=&arnumber=30651

[31] "Field Regions," [Online]. Available http://www.antenna-theory.com/basics/fieldRegions.php

[32] P. S. Nakar, "Design of a compact microstrip patch antenna for use in wireless/cellular devices," M.S. thesis, Dept. Elect. Comp. Eng. Florida State Univ., Tallahassee, FL, 2004.

[33] "Field Regions around an antenna," [Online]. Available http://www.giangrandi.ch/electronics/anttool/regions.shtml

[34] "Introduction to patch antennas," Antenna Theory [Online]. Available http://www.antenna-theory.com/

[35] C. A. Balanis, *Antenna Theory: Analysis and Design*, New York, NY: John Wiley & Sons, 1997.

[36] M. G. Lubner, C. L. Brace, J. L. Hinshaw, and F. T. Lee Jr, "Microwave Tumor Ablation: Mechanism of Action, Clinical Results and Devices," J. Vasc. Inverv. Radiol, 2011. [Online] Available http://www.ncbi.nlm.nih.gov/pmc/articles/PMC3065977/

[37] "Tissue Properties," [Online]. Available http://www.niremf.ifac.cnr.it/tissprop/

[38] E. Topsakal, “Antennas for medical applications: ongoing research and future challenges,” in International Conference on Electromagnetics in Advanced Applications, 2009, pp. 890-893.

[39] D. Yang, M. C. Converse, D. M Mahvi, and J. G. Webster, “Measurement and analysis of tissue temperature during microwave liver ablation,” *IEEE Trans. Biomed. Eng.*, vol. 54, pp. 150-155, Jan. 2007.

[40] Yang D, Converse MC, Mahvi DM, Webster JG., “Measurement and analysis of tissue temperature during microwave liver ablation.” IEEE Trans Biomed Eng 2007; 54:150–155.